Isobar production in $\pi^- p \to \pi^+ \pi^- n$ near threshold

R. A. Arndt, J. B. Cammarata, Y. N. Goradia,* R. H. Hackman, and V. L. Teplitz†
Department of Physics, Virginia Polytechnic Institute and State University, Blacksburg, Virginia 24061

D. A. Dicus
Center for Particle Theory, University of Texas, Austin, Texas 78712

R. Aaron
Department of Physics, Northeastern University, Boston, Massachusetts 02115

R. S. Longacre
Brooklyn National Laboratory, Upton, New York 11973

(Received 19 March 1979)

An isobar-model partial-wave analysis of 4140 $\pi^- p \to \pi^+ \pi^- n$ bubble-chamber events at total center-of-mass energies between 1330 and 1380 MeV is reported. Included in the analysis is a chiral-symmetry background calculated from the phenomenological Lagrangian. Significant results of the analysis are that production is dominated by the initial $P11$ wave and that, in this wave, final-state ϵN production is more important than $\pi\Delta$ production. We show that the recent single-arm-spectrometer data confirm the bubble-chamber data, where the two overlap. We discuss the determination of the chiral-symmetry-breaking parameter ξ. The analysis establishes that the present data is consistent with several models of the symmetry breaking, although it favors the vector breaking model of Weinberg, $\xi = 0$. Using a dispersion relation we show that ϵN production in the tail of the Roper ($P11$) resonance significantly affects the extraction of ξ from total-cross-section data; hence in pion production ξ cannot be determined independently of the isobar amplitudes. As a further application of the results of the analysis we determine the value of the $\Delta\pi\Delta$ coupling constant. Our result depends on the value taken for the Δ mass and what assumptions one makes to determine the large $\pi\Delta$ amplitudes; but, in any case, it is considerably less than the theoretical predictions which follow from SU(6), U(12), the quark model, and superconvergence relations. We also perform, in this paper, a Goldberger-Treiman–MIT-bag-model calculation which agrees with the other theoretical predictions. We further show that by attributing all $P33$ inelasticity to $\pi\Delta$ production the results of a recent elastic-phase-shift analysis imply upper bounds on the $\Delta\pi\Delta$ coupling constant which are consistent with the value implied by the isobar analysis.

I. INTRODUCTION

Low-energy single-pion production is a rich source of information on a number of important questions including (1) the validity of three-body equations, (2) the accuracy of theoretical predictions of resonance-resonance-particle couplings, and (3) the determination of deviations from chiral symmetry.

The world data set for the process comprises early emulsion experiments in the 50's and 60's,[1] bubble-chamber experiments from the 60's and 70's that yielded a total of about 300 000 events spread over the energy range 1300–2100 MeV[2,3] and, most importantly, a new wave of spectrometer experiments beginning in the later 70's with the LASL experiment of Gram *et al.*[4] at six energies from 1260 to 1360 MeV. Past isobar-model analyses of the data include the pioneering full-amplitude fit to the emulsion data by Olsson and Yodh,[5] an ambitious partial-wave analysis of two-thirds of the bubble-chamber data by a Berkeley-SLAC collaboration,[6] and subsequent analyses of partial data sets by workers at Saclay,[7] Imperial College,[8] and Caltech.[9]

The purpose of the present paper is, in general, to make contact between the bubble-chamber data and the spectrometer experiment[4] and, in particular, to present the conclusions that can be drawn from the lower-energy bubble-chamber data. About 4000 $\pi^- + p \to \pi^+ + \pi^- + n$ bubble-chamber events below 1380 MeV are available.[3] They divide fairly naturally into energy bins with $W = 1340 \pm 10$, 1360 ± 10, and 1375 ± 5 MeV. There are, of course, complete kinematics for each event. The spectrometer experiment detects, with good precision, the energy (E_+) and angle (θ_+) of just the π^+ over a fairly wide range of E_+ and z_+ ($= \cos\theta_+$) at six energies,

$W = 1260$, 1280, 1300, 1305, 1335,

and 1355 MeV.

In Sec. II we review the bubble-chamber data and, to facilitate comparison with the spectrometer experiment,[4] give the (E_+, z_+) distribution; the bubble-chamber distribution appears to be in good agreement with the counter data.

In Sec. III we turn to the question of chiral symmetry and chiral-symmetry breaking in the phenomenological-Lagrangian approach to $\pi N \to \pi\pi N$. This has been discussed in detail by several authors.[10-14] As the four-momenta of all three pions go to zero, chiral symmetry makes a unique prediction for the scattering amplitude in terms of the pion decay constant. The breaking of chiral symmetry is partially fixed by the value of the pion mass, but introduces one new parameter (ξ) which describes the tensor transformation property of the term in the Lagrangian that breaks the symmetry. The predictions of broken chiral symmetry are incorporated in the tree diagrams of a phenomenological Lagrangian.[11] In Sec. III we give these predictions. We also compare the predictions of the full phenomenological Lagrangian with that of its threshold approximation; the result is that they agree, for the chiral-symmetric part. The chiral-symmetry-breaking term, however, changes considerably with energy.

In Sec. IV we fit the bubble-chamber data. We use the chiral-symmetry prediction as a background and add the following isobar production amplitudes: $PP11(\pi\Delta)$, $PS11(\epsilon N)$, $PP33(\pi\Delta)$, $DS13(\pi\Delta)$, $DP13(\epsilon N)$, and $DS33(\pi\Delta)$. The (standard) notation here is [L (initial), L (final), total I, total J]. We also add what is left of the chiral-symmetry-breaking term after subtracting its projection onto $PS11(\epsilon N)$ and $DP13(\epsilon N)$; the latter is done to prevent a double counting of these production amplitudes. Our results are: (1) $PS11(\epsilon N)$ production is the largest single contribution; (2) $PP11(\pi\Delta)$ production is also large; (3) $PP33(\pi\Delta)$ production is surprisingly small; (4) $DS13(\pi\Delta)$ and $DP13(\epsilon N)$ production are approximately degenerate and definitely nonzero; (5) $DS33(\pi\Delta)$ production is probably not consistent with zero; and (6) the chiral-symmetry-breaking parameter ξ is consistent with zero. Zero for ξ implies that the σ commutator has a pure isotopic scalar ($I=0$) structure as would be expected in the quark model and that the symmetry-breaking term in the Lagrangian transforms like the "time" component of a chiral four-vector, in accordance with the model of Weinberg.[15]

In Sec. V we discuss an evaluation of the $\Delta\pi\Delta$ coupling constant using the results of our analysis. Our method is to study the diagram for $\pi N \to \Delta \to \pi\Delta \to \pi\pi N$. We first evaluate the cross section for this process using the amplitudes determined within the partial-wave isobar model. Then we evaluate the diagram using Lagrangian field theory, taking care to include spin complications for off-mass-shell Δ's. Comparing the two results yields our prediction $g_{\Delta\pi\Delta}{}^2/4\pi = 40 \pm 20$. This value disagrees with the predictions of SU(6) and a Goldberger-Treiman-type calculation. The latter agree with each other ($g_{\Delta\pi\Delta}{}^2/4\pi \simeq 100$) and are about 3 standard deviations higher than the result of the analysis.

In the concluding discussion of Sec. VI we compare our results with those of Herndon *et al.*[6] To check our result that $\xi = -0.3 \pm 1.6$, we consider a dispersion relation for the $PS11(\epsilon N)$ amplitude. From an approximate evaluation of the dispersion relation for the production amplitude near the three-body threshold we are able to conclude that the data tend to favor a value for ξ that is close to zero. Finally, we present a summary of the principal findings of this work.

II. "THRESHOLD" BUBBLE-CHAMBER DATA

In Fig. 1 we show the full world set of bubble-chamber data[2,3] below 2000 MeV for the four processes

1. $\pi^- p \to \pi^+\pi^- n$, 121 490 events,
2. $\pi^- p \to \pi^0\pi^- p$, 72 346 events,
3. $\pi^+ p \to \pi^0\pi^+ p$, 68 976 events,
4. $\pi^+ p \to \pi^+\pi^+ n$, 7460 events.

We note also that there are some recent data[16] on the reaction $\pi^- p \to \pi^0\pi^0 n$. For the present analysis we consider only the 4140 $\pi^- p \to \pi^+\pi^- n$ events below 1380 MeV.[3] The events have been centralized to the three total energy values 1340 ± 10 (1227 events), 1360 ± 10 (1481 events), and 1375 ± 5 (1432 events) using a scaling procedure. The latter is based on the relation between the square of subenergies s_i ($s_1 = s_{\pi^- n}$, $s_2 = s_{\pi^+ n}$, $s_3 = s_{\pi^+\pi^-}$) and the total c.m. energy squared s,

$$m^2 + 2m_\pi{}^2 = \sum_{i=1}^{3} s_i - s \,, \tag{2.1}$$

where m denotes the mass of the nucleon. We centralized by writing $s_i = s_i(\text{threshold}) + \Delta s_i$ and scaling, for a given event, the three Δs_i's by the same factor. Any events that fall outside the Dalitz plot are brought back by adding a few tenths of an MeV/c to the appropriate momentum.

In Figs. 2(a), 2(b), 2(c) we display the distributions of all 4140 events as functions of each of the three subenergies. The distributions for each set of centralized events are similar to those shown. One notes the strong peaking of the $\pi^+\pi^-$ energy s_3 toward high values, which shows the influence of the ϵ enhancement.

In the c.m. frame we define a coordinate system (Fig. 3) in which the initial-state nucleon is directed along the positive z axis and the momentum vector of the final nucleon defines the x-z plane. Letting z_+ (z_-, z_n) equal the cosine of the angle between the $+z$ axis and the π^+ (π^-, n) mo-

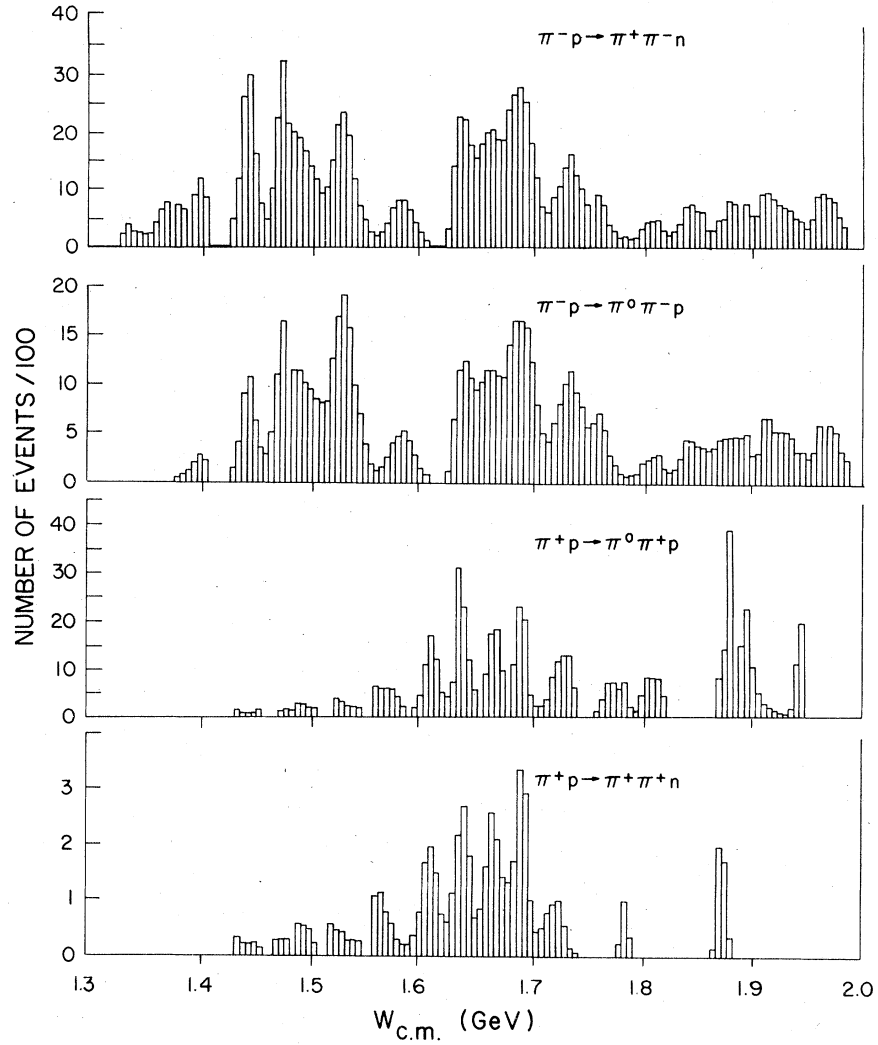

FIG. 1. Histograms of the available bubble-chamber data for $\pi^- p \to \pi^+ \pi^- n$, $\pi^- p \to \pi^0 \pi^- p$, $\pi^+ p \to \pi^0 \pi^+ p$, and $\pi^+ p \to \pi^+ \pi^+ n$.

mentum vector, we obtain for the full data set the angular distributions shown in Fig. 4. (Again, the results are the same at each of the three different energies.) Important features of the distributions are the ($z = -1$) π^+ and ($z = +1$) π^- peaking. These are opposite from the distributions one would expect on the basis of a simple one-pion-exchange model.

In Figs. 5(a), 5(b), 5(c) we give the distributions in (E_+, z_+) of the bubble-chamber events. (We have divided the plane into 10 energy bins and 10 cosine bins.) It is this distribution that the spectrometer experiment measures. The distribution can be fit by a function of the form

$$f(E_+, z_+) = A + CTz_+ + D(T_{\max} - T)z_+ + ET^2 , \quad (2.2)$$

where $T = (E_+ - m_\pi)/100$ and all quantities refer to the overall c.m. The values for the four parameters at the three energies are given in Table I. This parametrization is the same as that used by Gram *et al.*[4] in a preliminary analysis, and the values in Table I are in good agreement with their results.

III. BROKEN CHIRAL SYMMETRY

A. General theory

The general theory of broken chiral symmetry has been reviewed by many authors.[15,17,18] It has been applied to pion production by Chang,[10] Olsson and Turner,[11] Long and Kovacs,[12] Rockmore,[13] and Lomon.[14] We follow the general treatment of Weinberg[15] and the application to pion production of Olsson and Turner.[11] The basic idea is that, in the symmetry limit, S-matrix elements must be invariant under both isospin rotations and chiral "boosts" of chiral tensors, such as the chiral four-vector

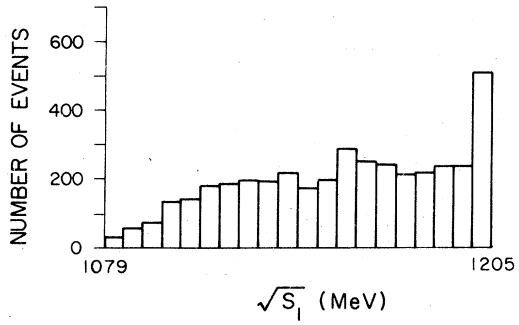

(a)

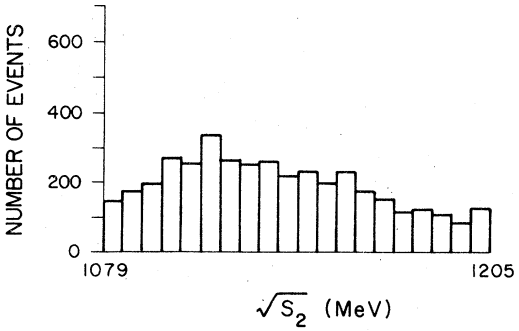

(b)

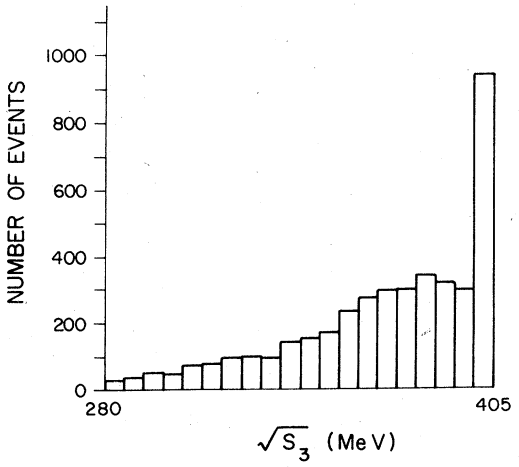

(c)

FIG. 2. Histograms of the bubble-chamber data used in this analysis (Ref. 3) as a function of the three invariant subenergies $\sqrt{s_1}$ (a), $\sqrt{s_2}$ (b), and $\sqrt{s_3}$ (c), as defined in the text. We plot $\sqrt{s_1}$ and $\sqrt{s_2}$ over the range 1079 to 1205 MeV and $\sqrt{s_3}$ over the range 280 to 405 MeV. Each bin is 6.25 MeV wide. For each graph the bin at the uppermost energy contains all events for $W = 1330 - 1380$ MeV that have a subenergy greater than the maximum energy shown on the graph.

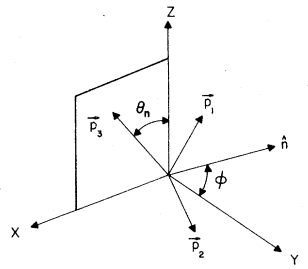

FIG. 3. The c.m. coordinate system. The momentum of the initial nucleon defines the $+z$ axis and the momentum ($\vec{p}_3$) of the final-state nucleon defines the x-z plane. $\vec{p}_1$ and $\vec{p}_2$ are the momenta of the final state π^+ and π^-, respectively, and n lies along $\vec{p}_1 \times \vec{p}_2$.

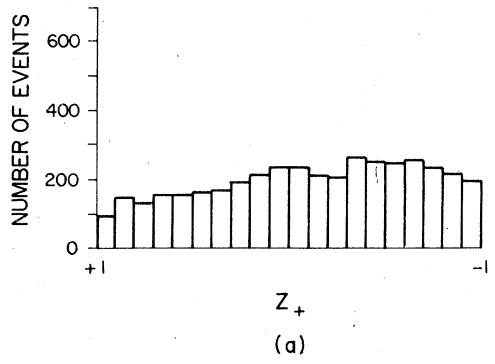

(a)

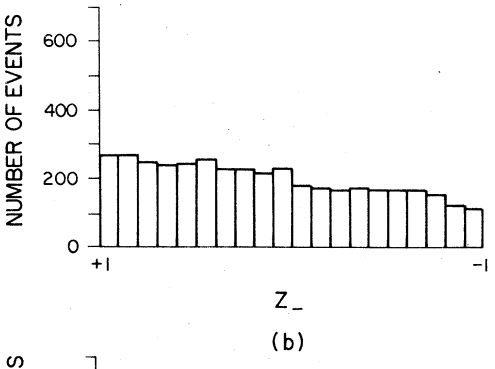

(b)

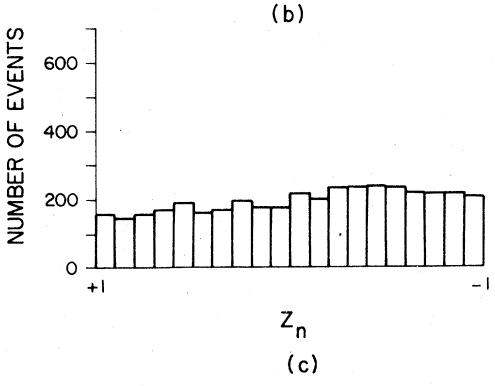

(c)

FIG. 4. Histograms of the angular variation of the 4140 bubble-chamber events used in the present analysis. The angular variables z_+, z_-, and z_n equal, respectively, the cosine of the angle between the z axis (cf. Fig. 3) and the π^+, π^-, and n momentum vectors. (The initial nucleon momentum is along the $+z$ axis.)

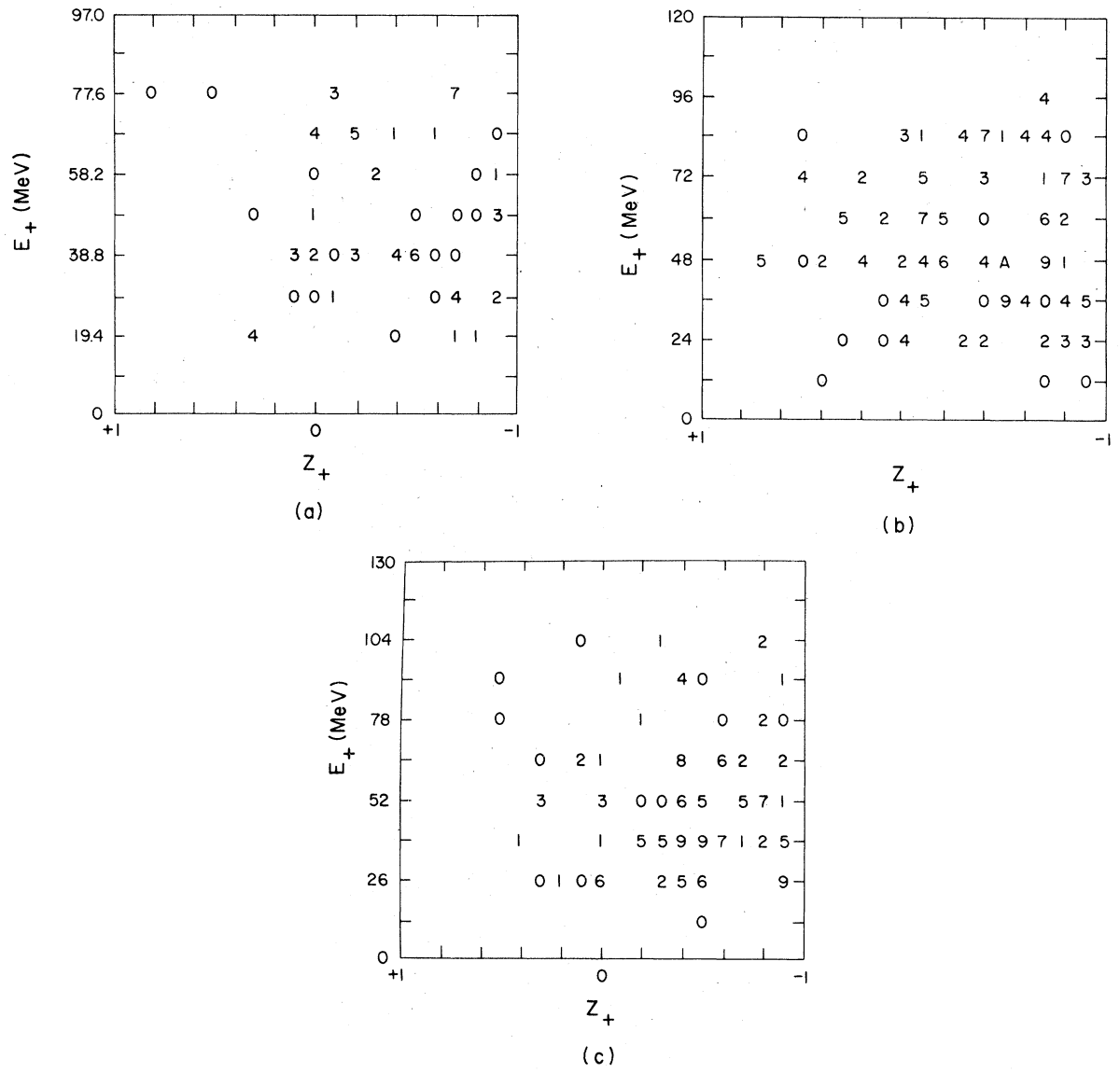

FIG. 5. Distributions in (E_+, z_+) of the bubble-chamber events at the three energies (a) 1340 ± 10 MeV, (b) 1360 ± 10 MeV, and (c) 1375 ± 5 MeV. E_+ is the π^+ kinetic energy in the overall c.m. We have divided the plane into 10 energy bins and 10 cosine bins. The relative number of events in each bin is given using an alphanumeric scale: $0 \to 9$, $A \to Z$, with 0 representing the smallest number of events.

TABLE I. Parameters for the phenomenological form, Eq. (2.2), for the distributions in (E_+, z_+) of the bubble-chamber events.

W (MeV)	A	C (MeV^{-1})	D (MeV^{-1})	E (MeV^{-2})
1340	22.12 ± 0.30	1.41 ± 0.64	-5.94 ± 0.58	-5.67 ± 0.50
1360	21.92 ± 0.28	0.30 ± 0.68	-4.14 ± 0.60	-7.51 ± 0.57
1375	20.81 ± 0.33	0.52 ± 0.95	-5.81 ± 0.89	-7.58 ± 0.99

$$[(c^2-\vec{\phi}^2)^{1/2},\ \vec{\phi}] \tag{3.1}$$

formed from the pion field $\vec{\phi}$ and any constant c. This invariance requirement summarizes the content of the current-algebra commutation relations

$$\begin{aligned}
&[V_\alpha^0(x), V_\beta^\mu(y)]_{x_0=y_0} = i\delta^3(\vec{x}-\vec{y})\epsilon_{\alpha\beta\gamma}V_\gamma^\mu(x) + \text{S.t.}\,,\\
&[A_\alpha^0(x), V_\beta^\mu(y)]_{x_0=y_0} = i\delta^3(\vec{x}-\vec{y})\epsilon_{\alpha\beta\gamma}A_\gamma^\mu(x) + \text{S.t.}\,,\\
&[V_\alpha^0(x), A_\beta^\mu(y)]_{x_0=y_0} = i\delta^3(\vec{x}-\vec{y})\epsilon_{\alpha\beta\gamma}A_\gamma^\mu(x) + \text{S.t.}\,,\\
&[A_\alpha^0(x), A_\beta^\mu(y)]_{x_0=y_0} = i\delta^3(\vec{x}-\vec{y})\epsilon_{\alpha\beta\gamma}V_\gamma^\mu(x) + \text{S.t.}\,,
\end{aligned} \tag{3.2}$$

(where S.t. stands for possible Schwinger terms) as applied to soft pions.

Predictions of the current algebra (3.2), with the PCAC (partial conservation of axial-vector current) condition that the pion pole dominate all matrix elements of the axial-vector current, can be reproduced by using a chiral-invariant Lagrangian constructed from covariant [in the sense of (3.1)] derivatives. The covariant derivative of the pion field is expressed in terms of the pion decay constant f_π as

$$D_\mu\vec{\phi} = (1+\tfrac{1}{4}f_\pi^{-2}\vec{\phi}^2)^{-1}\partial_\mu\vec{\phi}\,, \tag{3.3}$$

and for a field ψ with isospin operator $\vec{t}$ (for us ψ will be the nucleon)

$$D_\mu\psi = \partial_\mu\psi + 2i\tfrac{1}{4}f_\pi^{-2}(1+\tfrac{1}{4}f_\pi^{-2}\vec{\phi}^2)^{-1}\vec{t}\cdot(\vec{\phi}\times\partial_\mu\vec{\phi})\psi\,. \tag{3.4}$$

One can build a chiral-invariant Lagrangian by coupling $D_\mu\psi$, ψ, and $D_\mu\vec{\phi}$ in any isospin-invariant way. Such a Lagrangian, however, will have no mass term for the pion. This term is included in the symmetry-breaking part of the Lagrangian. As shown by Weinberg,[15] this term can be written as a power series in $f_\pi^{-2}\vec{\phi}^2/4$

$$\mathcal{L}_N = -\tfrac{1}{2}m_\pi^2\vec{\phi}^2\{1-\tfrac{1}{5}[N(N+2)+2]\tfrac{1}{4}f_\pi^{-2}\vec{\phi}^2+\cdots\}\,, \tag{3.5}$$

where N is the rank of the tensor operator as which $\mathcal{L}_N$ transforms under a chiral rotation. The $\pi\pi$ s-wave scattering lengths are related to N by

$$2a_0 + a_2 = \tfrac{3}{5}L[N(N+2)+2]\,, \tag{3.6}$$

where $L = m_\pi/8\pi f_\pi^2$. Specification of N fixes both scattering lengths since a second combination of a_0 and a_2,

$$2a_0 - 5a_2 = 6L\,, \tag{3.7}$$

is independent of any other parameters.

Specializing to $\pi N \to \pi\pi N$, we write the relevant π-N interaction terms for the chiral Lagrangian, following Ref. 11, as

$$\mathcal{L}_{NN\pi} = \frac{g_\pi}{2m}\bar{\psi}\gamma_\mu\gamma_5\vec{\tau}\psi\cdot\partial^\mu\vec{\phi}\,, \tag{3.8}$$

$$\mathcal{L}_{NN\pi\pi} = -\frac{g_\pi}{2m}\frac{1}{4f_\pi^2}\bar{\psi}\gamma_\mu\gamma_5\vec{\tau}\psi\cdot(\partial^\mu\vec{\phi})\vec{\phi}^2\,, \tag{3.9}$$

$$\mathcal{L}_{NN\pi\pi} = -\frac{1}{4f_\pi^2}\bar{\psi}\left[\gamma_\mu + i\frac{\kappa_V}{2m}\sigma_{\mu\nu}(p_f-p_i)^\nu\right]\vec{\tau}\psi\cdot(\vec{\phi}\times\partial^\mu\vec{\phi})\,, \tag{3.10}$$

$$\mathcal{L}_{\pi\pi} = -\frac{1}{4f_\pi^2}[\vec{\phi}^2(\partial^\mu\vec{\phi})^2 - \tfrac{1}{2}(1-\tfrac{1}{2}\xi)m_\pi^2(\vec{\phi}^2)^2]\,. \tag{3.11}$$

These terms are the same as those used in several other calculations[11-15,18,19] except for the anomalous-magnetic-moment term ($\kappa_V = 1.85$) in (3.10). This term plays a negligible role in the analysis, as discussed below. The pion decay constant and g_π are related to the weak axial-vector vertex function by the Goldberger-Treiman condition[20] $f_\pi g_\pi = m g_A(0)$, where we use $g_A(0) = 1.25$, $g_\pi = 13.5$, $m = 939$ MeV, and $f_\pi = 87$ MeV. ξ is related to the tensor rank N by

$$\xi = \tfrac{2}{5}[3 - N(N+2)]\,. \tag{3.12}$$

It measures the amount of departure from the assumption that that σ commutator is proportional to the σ field.[21] Using Eqs. (3.8)–(3.11) we find to order $\vec{\phi}^2$

$$[Q_5^\alpha, \partial^\mu A_\mu^\beta] = if_\pi m_\pi^2[\delta^{\alpha\beta}(f_\pi - \vec{\phi}^2/2f_\pi) + (\xi/4f_\pi)(\delta^{\alpha\beta}\vec{\phi}^2 + 2\phi^\alpha\phi^\beta)]\,, \tag{3.13}$$

where $f_\pi - \vec{\phi}^2/2f_\pi$ is the σ field to order $\vec{\phi}^2$. From (3.13) it also follows that ξ is a measure of the isotopic $I=2$ component of the σ commutator. If ϵ is the ratio of the $I=2$ to $I=0$ components, then[22]

$$\xi = \frac{18\epsilon}{15\epsilon - 6}\,. \tag{3.14}$$

In the following section we describe our procedure for determining ξ from a maximum-likelihood analysis of the data discussed in Sec. II. In addition to our analysis there are several theoretical models and experimental results from which ξ may be determined. In the general model of chiral-symmetry breaking of Gell-Mann, Oakes, and Renner[23] the nonsymmetric part of the Hamiltonian is assumed to transform according to the $(3,\bar{3})+(\bar{3},3)$ representation of SU(3)×SU(3). A prediction of the model is that $\xi = 0$. This and other predictions are based upon simple SU(3) assumptions involving certain chiral-symmetry-breaking meson matrix elements. However, it has been argued[24] that these assumptions have no *direct* relation to the quark model, so the latter can provide another, somewhat independent estimate of ξ. In the quark language, the σ commutator is expressed in terms of spinors for the "up" and "down" quarks and their average mass, $\hat{m}$, as[24]

$\hat{m}(\bar{u}u + \bar{d}d)$. This structure implies that the isotensor part of the commutator is zero, hence $\xi = 0$. Still further theoretical support for this value comes from the so-called hard-pion current-algebra method.[22,25] Here it is assumed that intermediate-state sums are saturated by low-lying single-meson states. Within the pole dominance approximation, the assumption that there is no $I=2$ component to the σ commutator is natural as there are no known $I=2$ s-wave $\pi\pi$ resonances.

Aside from $\pi N \to \pi\pi N$, another reaction from which ξ may be extracted is the decay $K^\pm \to \pi^+\pi^- e^\pm \nu_e$. From the analysis of several experiments on K_{e4} decay, various values of the $I=0$, s-wave $\pi\pi$ scattering length a_0 have been determined.[26] Hite and Jacob[27] have also recently applied interior dispersion relations to πN scattering amplitudes to extract a_0. An average of these results is

$$a_0 = 0.25 \pm 0.09 m_\pi^{-1}. \tag{3.15}$$

Using Eqs. (3.6), (3.7), (3.12) and $f_\pi = 87$ MeV, this implies $-2.53 \leq \xi \leq 0.29$, which is consistent with the theoretical predictions. In this regard one should note that Weinberg's[28] original calculation of the $\pi\pi$ scattering lengths was based on the assumption that the σ commutator was pure isoscalar, so his result is in agreement with (3.15). The scattering length also agrees with the recent symmetry-breaking model of Schwinger,[19] which implies that $\xi = -2$.

B. Predictions for pion production

From (3.8)–(3.11) one may calculate the amplitude $T(\pi N \to \pi\pi N)$ for the diagrams of Fig. 6. In Appendix A we give the complete results for all the tree diagrams for all independent pion production processes without making any threshold approximation in the kinematics.

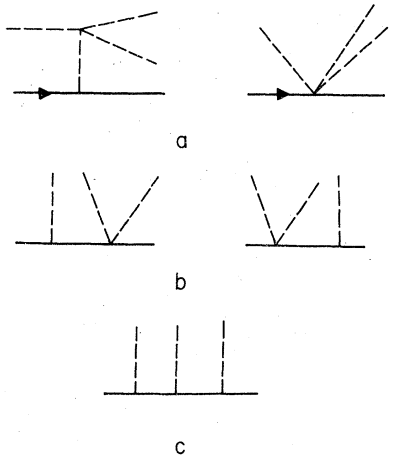

FIG. 6. Tree diagrams which contribute to the process $\pi N \to \pi\pi N$. (a) includes the "one-point," (b) the "two-point," and (c) the "three-point" diagrams.

The total cross section predictions of these amplitudes are presented in Fig. 7 for both $\xi = 0$ and $\xi = -2$. For comparison, in Fig. 7(a) we also show the prediction of the anomalous-magnetic-moment term (for $\pi^- p \to \pi^+\pi^- n$), which arises from the second term in (3.10). The contribution to other charge states is of comparable importance, and in our final fitting we did not include this term.

The amplitudes generated with a chiral Lagrangian are expected to be valid only through terms linear in the pion momenta—terms of higher order may be strongly model dependent.[18] In the present analysis, we have used the full amplitude. To test the model dependence of the ξ-independent piece of our amplitude, we expanded numerically $T(\pi N \to \pi\pi N)$ in a power series in the pion momenta and retained only linear terms. The deviation of the cross-section predictions of this threshold amplitude from those of the full amplitude (see Fig. 7) are a measure of the significance of the model dependence of our results. This numerical expansion is effected as follows. First, we scale the three-momenta of the final state pions $\vec{q}_1$ and $\vec{q}_2$, by a parameter $\rho \ll 1$; and then we form the symmetric and antisymmetric parts of $T(\pi N \to \pi\pi N)$ in q_1 and q_2. This threshold approximation to the ξ-independent part of the amplitude is evaluated at the appropriate energy according to

$$T_{\rm th} = T_{\rm th}^{(+)} + T_{\rm th}^{(-)}, \tag{3.16}$$

where we write

$$T_{\rm th}^{(+)} = \frac{1}{2}\left[T(\rho\vec{q}_1, \rho\vec{q}_2) + T(\rho\vec{q}_2, \rho\vec{q}_1)\right]\frac{|\vec{Q}|}{|\vec{Q}_{\rm th}|}, \tag{3.17}$$

$$T_{\rm th}^{(-)} = \frac{1}{2\rho}\left[T(\rho\vec{q}_1, \rho\vec{q}_2) - T(\rho\vec{q}_2, \rho\vec{q}_1)\right]. \tag{3.18}$$

Here, $\vec{Q}$ is the c.m. momentum of the incident pion, $\vec{Q}_{\rm th}$ is the threshold value of $\vec{Q}$, and ρ is the scaling factor. The symmetric part of T is a threshold approximation appropriate to production of s-wave final-state pions, and the antisymmetric part, a threshold approximation appropriate to production of p-wave final-state pions. For the chiral-symmetry-breaking part of the production amplitudes, T_ξ, we use a symmetric threshold approximation

$$(T_\xi)_{\rm th} = \frac{1}{2}\left[T_\xi(\rho\vec{q}_1, \rho\vec{q}_2) + T_\xi(\rho\vec{q}_2, \rho\vec{q}_1)\right]\frac{|\vec{Q}|}{|\vec{Q}_{\rm th}|}. \tag{3.19}$$

In Fig. 7, we depict the cross-section predictions of (3.16) and (3.19) for both $\xi = 0$ and $\xi = -2$. We also present the predictions of a "hybrid" amplitude in which the threshold approximation de-

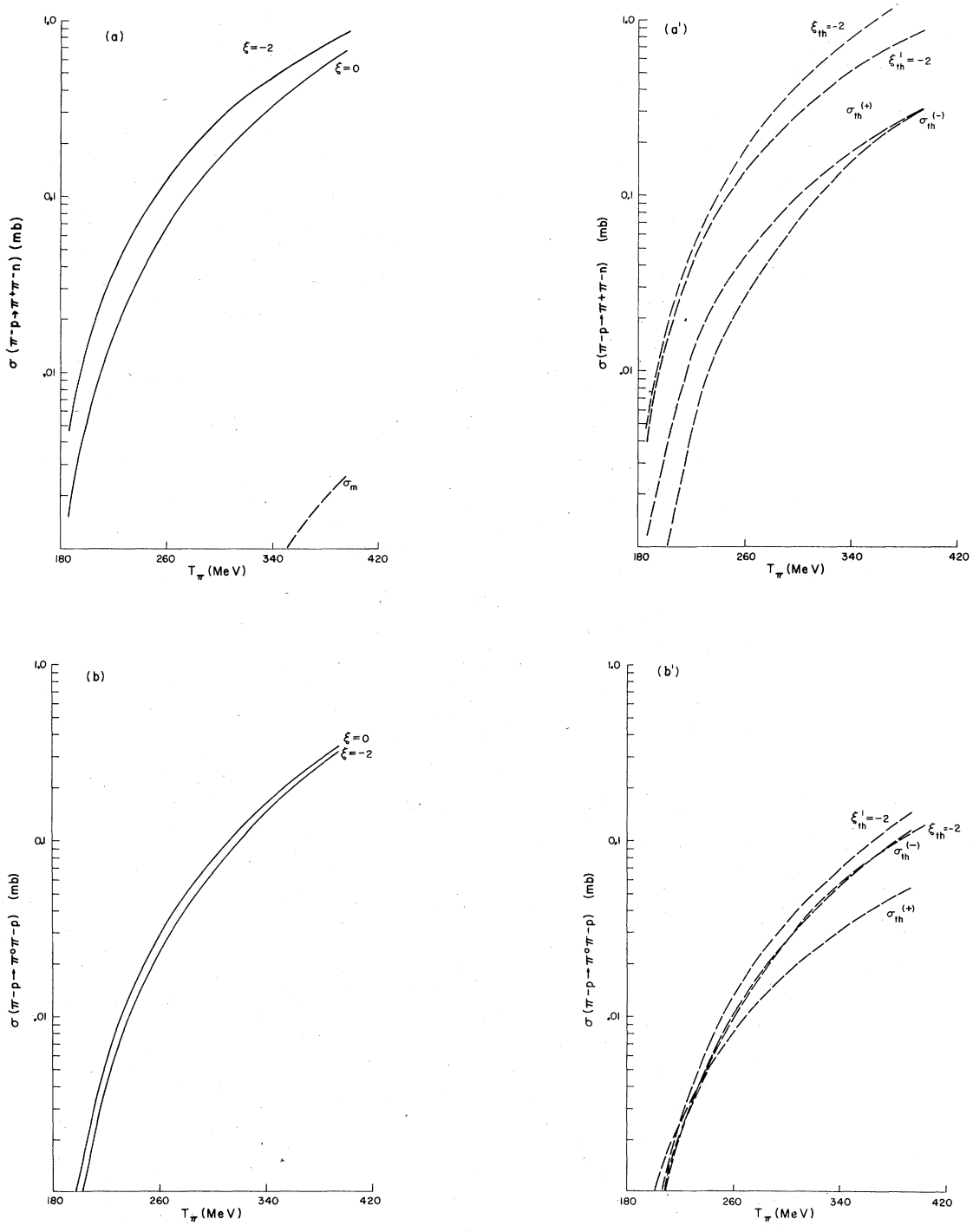

FIG. 7. The total-cross-section prediction of the chiral Lagrangian [Eqs. (3.8)–(3.11)] for (a) $\pi^-p \to \pi^+\pi^-n$, (b) $\pi^-p \to \pi^0\pi^-p$, (c) $\pi^+p \to \pi^0\pi^+p$, (d) $\pi^-p \to \pi^0\pi^0n$, and (e) $\pi^+p \to \pi^+\pi^+n$ for both the Weinberg ($\xi = 0$) and the Schwinger ($\xi = -2$) models. The curves labeled $\sigma_{\rm th}^{(+)}$ and $\sigma_{\rm th}^{(-)}$ in (a'), (b'), (c'), (d'), and (e') are the symmetric and antisymmetric threshold approximations to the cross section described and discussed in Sec. III. The curves labeled $\xi_{\rm th} = -2$ are the full threshold approximation to the Schwinger model and those labeled $\xi'_{\rm th} = -2$, the hybrid cross sections in which the threshold approximation is used only for the chiral-symmetric part of the amplitude. The threshold approximation to the Weinberg model is the sum of $\sigma_{\rm th}^{(+)}$ and $\sigma_{\rm th}^{(-)}$. In (a) σ_m is the total cross section which results from the anomalous term [in Eq. (3.10)].

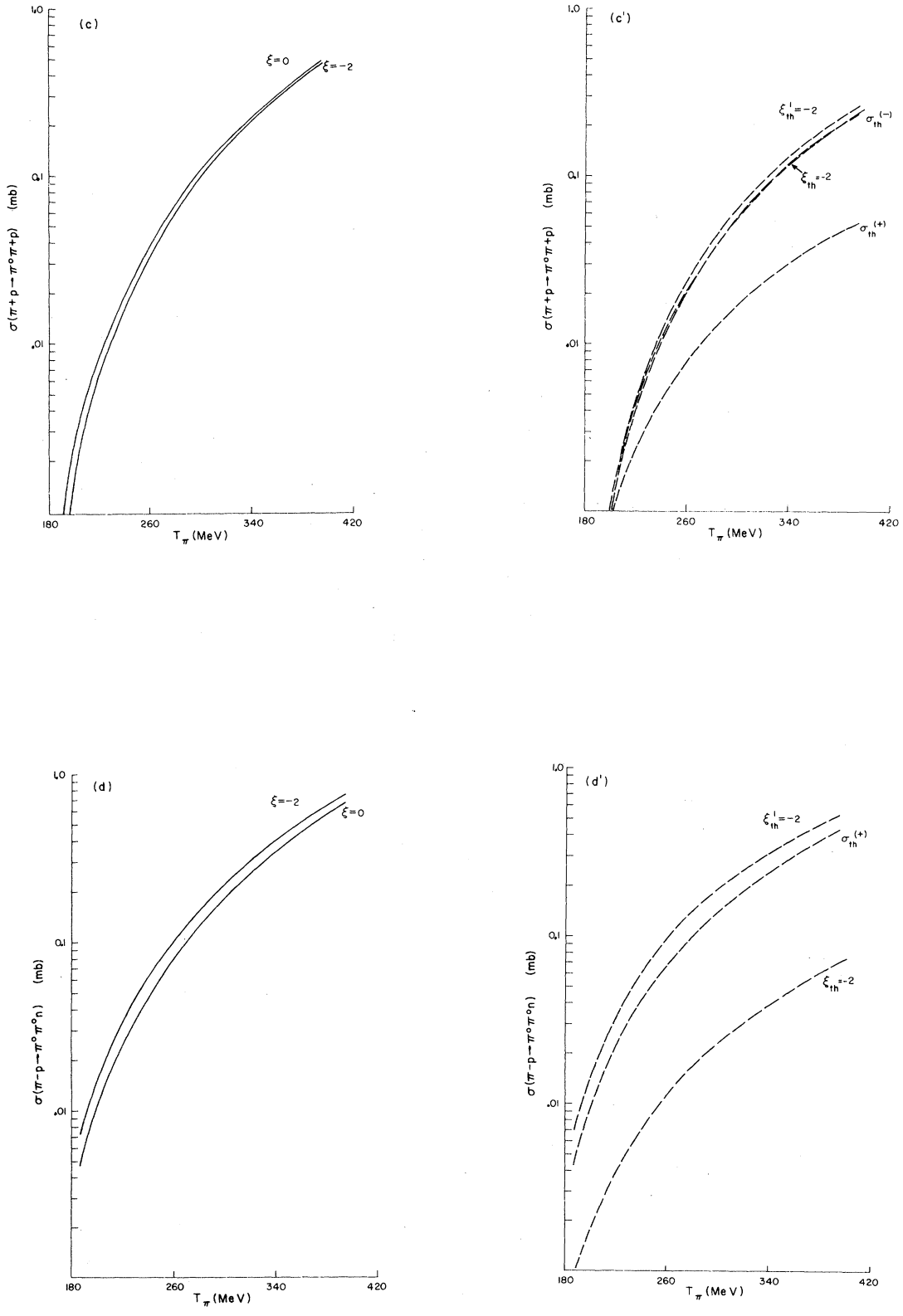

FIG. 7. (*Continued*).

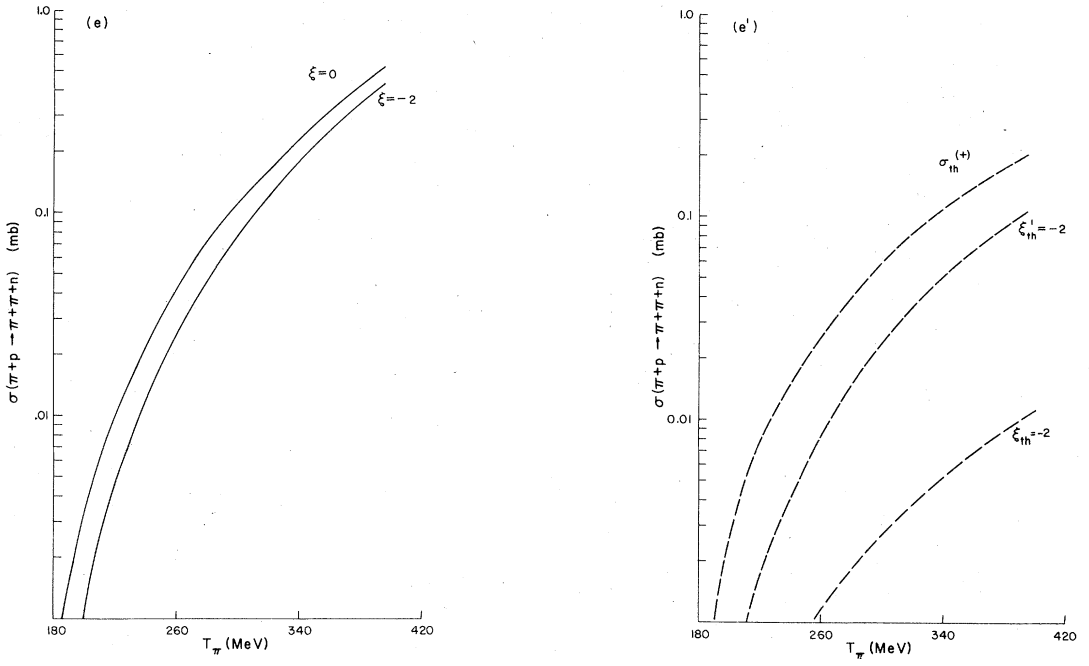

FIG. 7. (*Continued*).

scribed above is used only for the ξ-independent part of $T(\pi N \to \pi\pi N)$. For $\pi^- p \to \pi^+\pi^- n$, the $\xi = 0$ cross sections generated with this threshold approximation are virtually indistinguishable from those generated with the full amplitude. Although not conclusive, this implies that the ξ-independent part of our amplitude is model independent. The $\xi = -2$ predictions of T_{th}, however, are ~50% larger than the predictions of the full amplitude at the uppermost energies. For the remaining charge states, the differences between σ and σ_{th} indicates that the model dependence of even our chiral-symmetric predictions is likely to be significant.

C. Comparisons with previous analyses

The arguments in Sec. III A strongly support the Weinberg model of symmetry breaking ($\xi = 0$). However, the results of previous π-production analyses have not been definitive in this regard. For example, while Rockmore[13] concludes that the data are consistent with $\xi = 0$, the analyses of Long and Kovacs,[12] and more recently that of Lomon,[14] support the Schwinger model[19] ($\xi = -2$) in which the σ commutator has isoscalar and isotensor terms. In another recent analysis, Olsson, Osypowski, and Turner[11] find that $\xi = -0.8 \pm 0.4$ which is 2 standard deviations away from either model.

The proper assessment of the results of these analyses is complicated by the different approximations involved. Olsson, Osypowski, and Turner consider only the one- and two-point diagrams depicted in Fig. 6—the three-point graphs are neglected. Furthermore, they use a threshold approximation to the T matrix

$$T(\pi N \to \pi\pi N) \cong a(\pi N \to \pi\pi N)|\vec{Q}|\,, \tag{3.20}$$

where $\vec{Q}$ is the c.m. momentum of the incident pion and $a(\pi N \to \pi\pi N)$ is the T matrix evaluated at threshold divided by the threshold value of $|\vec{Q}|$. This threshold approximation is essentially our $T_{\text{th}}^{(+)} + (T_\xi)_{\text{th}}$ (the graphs neglected by Olsson, Osypowski, and Turner are small) and the curves labeled $\sigma_{\text{th}}^{(+)}$ in Fig. 7 reprduce the $\xi = 0$ cross-section predictions of these authors. In this regard, it should be noted that the figure depicting the total cross section for $\pi^- p \to \pi^+\pi^- n$ as a function of the pion laboratory kinetic energy, T_π, in the first of Ref. 11 is incorrect. However, the plot of $\vec{Q}^2$ $\times$phase space in the second of Ref. 11 is correct, as are the threshold expressions for the pion production amplitudes in both of these papers.

Rockmore[13] also uses the threshold approximation of Eqs. (3.16), (3.19) and considers π production from both single-nucleon and nuclear collisions. In the earlier Rockmore paper (the first of Ref. 13), it is noted that the ξ-dependent part of the effective Lagrangian for π production does not agree with the current commutator calculation of Chang.[10] Rockmore mistakenly concludes that the

TABLE II. The total-cross-section predictions (in mb) including both the chiral amplitude (with $\xi = 0$) and isobar production. The first number corresponds to the EPP solutions (Table V), the second (in parentheses) to the SPP solutions (Table VI). These solutions are discussed in Sec. IV. The cross sections are generated through a Monte Carlo calculation with 2000 points. We estimate (from Tables V and VI) that the errors on the total cross sections are about ±20%.

	1340 ± 10 MeV	1360 ± 10 MeV	1375 ± 5 MeV
$\pi^- p \to \pi^+ \pi^- n$	1.39	2.10	2.62
	(1.30)	(2.15)	(2.51)
$\pi^- p \to \pi^0 \pi^0 n$	0.75	1.15	1.42
	(0.73)	(1.12)	(1.34)
$\pi^+ p \to \pi^+ \pi^+ n$	0.27	0.44	0.61
	(0.30)	(0.52)	(0.63)
$\pi^- p \to \pi^0 \pi^- p$	0.19	0.32	0.49
	(0.21)	(0.33)	(0.48)
$\pi^+ p \to \pi^0 \pi^+ p$	0.26	0.63	0.72
	(0.34)	(0.71)	(0.98)

two approaches are not equivalent, the effective Lagrangian requiring $\xi = 0$ to be consistent with the available low-energy $\pi^- p \to \pi^+ \pi^- n$ data and the current commutator, $\xi = -\frac{1}{2}$. However, Olsson, Osypowski, and Turner (in the third of Ref. 11) later point out that the discrepancy between the two approaches is due to the neglect of certain pion pole diagrams in the current-commutator calculation. This last reference is the most current calculation which uses the threshold approximation; it gives $\xi = -0.8 \pm 0.4$, as noted earlier.

In the present analysis, aside from questions of the model dependence of T_ξ, we find that (3.16) is not a good approximation to the production amplitude at the energies at which data are present for two reasons. First, the threshold approximation of Olsson, Osypowski, and Turner neglects production of the two final-state pions in a relative p state. From Fig. 7, we see that for $\pi^- p \to \pi^+ \pi^- n$ the cross-section predictions of $T_{\rm th}^{(+)}$ ($\sigma_{\rm th}^{(+)}$) and of $T_{\rm th}^{(-)}$ ($\sigma_{\rm th}^{(-)}$) are of comparable importance at the relevant energies. Second, we find that isobar production makes an important contribution to the production cross section. Especially important is the interference between the ξ-dependent piece of the chiral amplitude and ϵN isobar channel as discussed below in Sec. IV C. In Table II, we present the total-cross-section predictions of our analysis. For $\pi^- p \to \pi^+ \pi^- n$, the chiral-symmetric amplitude accounts for only 20% to 30% of the total production cross section. It is apparently the use of the threshold approximation (3.20), particularly in regard to the chiral-symmetry-breaking piece, which allows the $T(\pi N \to \pi\pi N)$ used by Olsson, Osypowski, and Turner to compensate for the lack of isobar production and the neglect of $T_{\rm th}^{(-)}$ in their total-cross-section predictions at the energies considered by these authors.

Long and Kovacs[12] use the full amplitude as generated by the phenomenological Lagrangian of Eqs. (3.8)–(3.11) (excluding the small anomalous magnetic moment term), but neglect isobar production in their analysis. Using several different models for the symmetry breaking, these authors make predictions for total cross sections for $\pi^- p \to \pi^+ \pi^- n$, $\pi^+ p \to \pi^+ \pi^0 p$, and $\pi^- p \to \pi^- \pi^0 p$ and for certain differential cross sections for $\pi^+ p \to \pi^+ \pi^+ n$ and $\pi^- p \to \pi^+ \pi^- n$. In a comparison with data on these processes they find that $\xi = -2$ leads to the best agreement; however, our numerical work, as discussed below in Secs. IV F and VI B, implies that this result is inconclusive because of the neglect of isobar production.

IV. THE FIT TO THE BUBBLE-CHAMBER DATA

A. Introduction

We took the chiral-symmetry contribution to $\pi^- p \to \pi^+ \pi^- n$ from Eqs. (A12)–(A15), subtracted from the symmetry-breaking term in (A12) its $P11$ and $D13$ components, added production of what we consider to be the six potentially most important isobar states, and determined ξ and the six isobar production amplitudes from a maximum-likelihood analysis of the bubble-chamber data described in Sec. II. The details of this analysis are given below, while the results are summarized in Tables V–VIII.

B. Isobar production amplitudes

In Ref. 29 we gave in detail our formalism for determining partial-wave amplitudes in the isobar model. Here we reproduce the principal results in a form close to the actual programming. In Appendix B we give numerical examples. For the

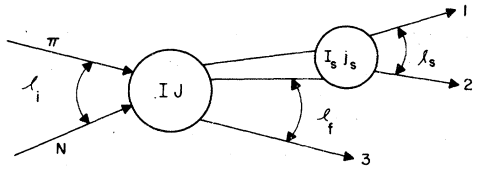

FIG. 8. Notation for the reaction $\pi N \to 1+2+3$ with a two-particle resonance in the final state.

isobar amplitude we write

$$T_{IM}=\sum_{\alpha} A_{\alpha'} X_{\alpha} , \tag{4.1}$$

where the index α is the collection

$$\alpha=\{I, I_s, i_\pi, i_N, i_1, i_2, i_3, J, l_i, l_f, l_s, \mu_i, \mu_f, j_s\} , \tag{4.2}$$

with i denoting an isospin projection and μ a spin projection. α' is the same set as α but without any projection quantum numbers. The indices in the collection (4.2) are defined in Fig. 8. In the present analysis we include only the ϵ and Δ isobars. The basis functions for these states are given by [$C(j_1 j_2 j; m_1 m_2 m)$ is a Clebsch-Gordan coefficient]

$$X_\epsilon=\sqrt{2}\,C(1\tfrac{1}{2}\tfrac{1}{2};i_\pi i_N i)C(110;i_1 i_2 0)C(\tfrac{1}{2} l_i J;\mu_i 0 \mu_i)C(\tfrac{1}{2} l_f J;\mu_f,\mu_i-\mu_f,\mu_i)$$
$$\times Y_{l_f,\mu_i-\mu_f}(\hat{p}_3)\left(\frac{2l_i+1}{4\pi}\right)^{1/2} W_3\left(\frac{e^{i\delta}\sin\delta}{q_3}\right)\frac{B_{\epsilon,l_f}(q_3)}{R_{\epsilon,l_f}} \tag{4.3}$$

and

$$X_\Delta^{(2)}=C(1\tfrac{1}{2} I;i_\pi i_N i)C(1\tfrac{1}{2}\tfrac{3}{2};i_1 i_3 i_\Delta)C(\tfrac{3}{2}1 I;i_\Delta i_2 i)C(\tfrac{1}{2} l_i J;\mu_i 0\mu_i)$$
$$\times\sum_m [C(\tfrac{1}{2}1\tfrac{3}{2};\mu_f m,\mu_f+m)C(\tfrac{3}{2} l_f J;\mu_f+m,\mu_i-(\mu_f+m),\mu_i)Y_{1m}(\hat{q}_2)Y_{l_f,\mu_i-(\mu_f+m)}(\hat{p}_2)]$$
$$\times\left(\frac{2l_i+1}{4\pi}\right)^{1/2}\left(\frac{4\pi}{3}\right)^{1/2} W_2\left(\frac{e^{i\delta}\sin\delta}{q_2^{\,2}}\right)\frac{B_{\Delta,l_f}(q_2)}{R_{\Delta,l_f}} . \tag{4.4}$$

$X_\Delta^{(2)}$ describes the case when the Δ is made up of particles 1 and 3 ($\pi^+ n$); there will also be a contribution $X_\Delta^{(1)}$ from the ($\pi^- n$) isobar. The two-body phase shifts, δ, for πN in the 3-3 state and $\pi\pi$ in the $I=J=0$ state are taken from the elastic analyses of Refs. 30 and 31, respectively. In the barrier penetration factors B, which are defined by Blatt and Weisskopf,[32] we set the radius equal to 0.25 fm. Our results will depend only very weakly on the radius value (for reasonable choices), and we note that for our value the penetration factors are essentially $B_{\alpha,l_f} \propto q^{l_f}$. The normalization integrals R are given by

$$R_{\epsilon,l_f}{}^2=h(W)\int\frac{\sin^2\delta_{\pi\pi}}{q_3}s_3 p_3 B_{\epsilon,l_f}{}^2 dW_3 , \tag{4.5}$$

$$R_{\Delta,l_f}{}^2=\tfrac{1}{3}h(W)\int\frac{\sin^2\delta_{\pi N}}{q_2^{\,3}}s_2 p_2 B_{\Delta,l_f}{}^2 dW_2 , \tag{4.6}$$

where

$$h(W)=p[32(2\pi)^6]^{-1}\left(\frac{m}{W}\right)^2 . \tag{4.7}$$

In our notation $\vec{p}_1$, $\vec{p}_2$, and $\vec{p}_3$ are the c.m. momenta of the π^+, π^-, and n, while $W_i=\sqrt{s_i}$ and q_i are the subenergy and relative momentum for the j-k pair [$(ijk)=(123)$ *et cycl.*]. $W=\sqrt{s}$ is the total c.m. energy, and p is the c.m. momentum for the initial state. Because of the ordering of factors in the Clebsch-Gordan coefficients in (4.3) and (4.4), our $A_{\alpha'}$'s will differ by various signs from those of Refs. 6, 7, and 8. Relevant sign conventions are discussed in detail in Sec. VI A.

C. Total production amplitudes

We fit the following six isobar production amplitudes:

$$PP11(\pi\Delta), PS11(\epsilon N),\ PP33(\pi\Delta),\ DS13(\pi\Delta),$$
$$DP13(\epsilon N),\ \text{and}\ DS33(\pi\Delta) .$$

Our criteria for these choices were: (1) we took all final-state s waves, and (2) we took final-state p waves arising from resonant initial states ($P33, P11, D13$). In relation to the extraction of the chiral-symmetry-breaking parameter, we also consider the $SP11(\epsilon N)$ wave, as discussed below. It should be noted that, even though our data are all in one charge channel ($\pi^+\pi^- n$), we can determine both $I=\frac{1}{2}$ and $I=\frac{3}{2}$ $\pi\Delta$ production amplitudes. This is because the relative amounts (and the relative signs) of the $\pi^+\Delta^-$ and $\pi^-\Delta^+$ contributions are different for the two isospin states.

In computing total cross sections in the isobar model it is necessary to include the overlaps between pairs of basis functions for production of different isobars from the same initial state. The size of the overlap is a measure of the nonorthogonality of the final states. All overlaps have been calculated in a previous work by two of us[33]

TABLE III. The normalized overlaps defined by Eq. (4.9) and the overlaps with the chiral-symmetric background. The integrals are computed with a Monte Carlo routine, using 5000 points. The overlaps involving Δ isobars were computed using $X_\Delta = X_\Delta^{(1)} + X_\Delta^{(2)}$.

(a) Normalized overlaps

W (MeV)	$PP11(\pi\Delta)$ × $PS11(\epsilon N)$	$DS13(\pi\Delta)$ × $DP13(\epsilon N)$	$DS13(\pi\Delta)$ × $DS33(\pi\Delta)$	$DP13(\epsilon N)$ × $DS33(\pi\Delta)$
1340	$0.22-0.06i$	$-0.84-0.19i$	0.60	$-0.21+0.05i$
1360	$0.25-0.06i$	$-0.78-0.29i$	0.60	$-0.19+0.07i$
1375	$0.22-0.04i$	$-0.73-0.36i$	0.59	$-0.17+0.07i$

(b) Overlaps with chiral-symmetric background

	1340 MeV	1360 MeV	1375 MeV
$PP11(\pi\Delta)$	$-0.5+0.2i$	$-0.5+0.3i$	$-0.6+0.3i$
$PS11(\epsilon N)$	$1.3-0.3i$	$1.4-0.4i$	$1.5-0.4i$
$PP33(\pi\Delta)$	$0.3-0.1i$	$0.3-0.1i$	$0.3-0.2i$
$DS13(\pi\Delta)$	$-1.0+0.5i$	$-1.1+0.7i$	$-1.1+0.9i$
$DP13(\epsilon N)$	$0.8-0.2i$	$0.9-0.3i$	$1.1-0.3i$
$DS33(\pi\Delta)$	$-0.7+0.3i$	$-0.8+0.5i$	$-0.7+0.6i$

and were rechecked by a different method in the present work. We define

$$X_{\alpha\beta} = \int X_\alpha^* X_\beta \, d\rho \,, \tag{4.8}$$

where ρ denotes the four-dimensional phase space. We note that the basis functions X_α $(=X_\epsilon, X_\Delta^{(1)}, X_\Delta^{(2)})$ are such that the partial-wave cross section has the form

$$\sigma_\alpha = 4\pi\lambda^2(J+\tfrac{1}{2})\left|A_{\alpha'}\right|^2 \times [\mathrm{CG\ (isospin)}_\alpha]^2 .$$

The normalized overlaps

$$\tilde{X}_{\alpha\beta} = X_{\alpha\beta}/(X_{\alpha\alpha}X_{\beta\beta})^{1/2} \tag{4.9}$$

are given in Table III for the waves of interest. Also shown are the overlaps with the chiral-symmetry background

$$B_\alpha = \int X_\alpha^* T_{\mathrm{CS}} \, d\rho \,. \tag{4.10}$$

We see from the table that the $PS11(\epsilon N)$ and $PP11(\pi\Delta)$ have a small overlap, while the $DS13(\pi\Delta)$ and $DP13(\epsilon N)$ have a very large one. Because of the latter feature, we were not able to make a clear separation of the two amplitudes. It should be noted, however, that the (normalized) overlap in the isobaric production cross section has a different value from the charge state one so that a good measurement of the total $D13$ reaction cross section would determine the relative amplitudes.

Equation (A12) suggests a total production amplitude T of the form

$$T = T_{\mathrm{CS}} + \xi T_\xi + \sum A_{\alpha'} X_\alpha \,, \tag{4.11a}$$

where T_{CS} is the "chiral-symmetry" part of the current-algebra amplitude, ξT_ξ a generalization of the chiral-symmetry-breaking part of the current-algebra amplitude, and we have added the term $\sum A_{\alpha'} X_\alpha$ to describe isobar production. The isobar sum includes the six waves mentioned earlier. Up to a constant, T_ξ is the "usual" one-pion exchange diagram given in Eq. (3.11) of Aaron *et al.*[29] It should be emphasized that the $A_{\alpha'}$ are not the full production amplitudes, but rather the deviations from current algebra.

At this point one would like to fit the data with ξ and the six $A_{\alpha'}$ as fitting parameters. Unfortunately, this is not possible. The reason is that according to Ref. 29, we may expand

$$T_\xi = \sum B_{\alpha'} X_\alpha \tag{4.11b}$$

where the $B_{\alpha'}$ are known, and below 1400 MeV, to a very good approximation, only three waves—$PS11(\epsilon N)$, $DP13(\epsilon N)$, and $SP11(\epsilon N)$—contribute to the cross section. The fitting procedure determines the coefficients of the basis functions, X_α. For the $PS11(\epsilon N)$ and $DP13(\epsilon N)$ waves, the $B_{\alpha'}$ of (4.11b) combine with the $A_{\alpha'}$ of (4.11a) giving new fitting parameters, and consequently these waves cannot determine ξ. It is only the coefficient of the $SP11(\epsilon N)$ basis vector, that appears in the expansions of T_{CS} and T_ξ but not in the α' sum in (4.11a), that can be used to determine the ξ parameter. Therefore, our procedure is, essentially, to identify ξ by the deviation of $SP11$ production from the chiral-symmetry prediction. It should

be noted that, in the threshold limit, T_ξ is pure $PS11$ because the energy denominator $[(p_f - p_i)^2 - m_\pi{}^2]$ has no $z_N = \hat{p}_f \cdot \hat{p}_i$ dependence. Our method depends on going far enough from threshold to make an appreciable $SP11$ component. The $SP11$ wave is particularly appropriate for this task because the absence of any (nearby) resonances implies that, of the large waves, it should be the least affected by unitarity corrections. We note that at 1360 MeV, T_ξ would give, with $\xi = -2$, approximately 1% of the observed cross section and would therefore make a 10% difference in the amplitude. Thus ξ could be measurable with the bubble-chamber data.

Since current algebra applies as all pion four-momenta go to zero, it would be desirable to determine ξ from the spectrometer data.[4] Unfortunately, single-arm spectrometer data determine only two of the four final-state kinematic variables and hence may not be amenable to a three-body, partial-wave analysis. It is therefore an uncertain tool for determining the extent of isobar production and hence the deviation of the remainder from the chiral-symmetry limit. It should be noted that the work of Nath and Kere[34] implies that ϵN production in the tail of the Roper resonance should persist at low energies. We find, as discussed in Sec. IV F, large ϵN production at 1340, 1360, and 1375 MeV; in Sec. VI B we discuss a dispersion relation calculation which estimates the rate at which the ϵN production decreases toward threshold. It is, of course, difficult to distinguish the $P11$- resonance tail ϵN production from the one-pion-exchange (OPE) pion production at low energy; thus, for a reliable determination of ξ one may need to fix the OPE contribution by means of nonresonant waves, as is done in the present work.

D. The fitting procedure

We use a maximum-likelihood procedure similar to that used by the Berkeley-SLAC collaboration and described in Ref. 6. The quantity that is minimized is χ^2, which is defined by

$$\chi^2 = 2N\left(\ln\bar{\sigma} + \frac{\sigma_T}{\bar{\sigma}}\right) - 2\sum_i \ln\sigma_i + \frac{(\bar{\sigma} - \sigma_x)^2}{(\Delta\sigma_x)^2}\,, \tag{4.12}$$

where N is the total number of event points, $\bar{\sigma}$ is the fitted cross section, and σ_x is the experimental total cross section with error $\Delta\sigma_x$. In our fitting we used the new total-cross-section values interpolated from Ref. 4 (with generous errors assumed)

$$\sigma_x \pm \Delta\sigma_x(1340) = 1.35 \pm 0.15 \text{ mb}\,, \tag{4.13a}$$

$$\sigma_x \pm \Delta\sigma_x(1360) = 2.25 \pm 0.20 \text{ mb}\,, \tag{4.13b}$$

$$\sigma_x \pm \Delta\sigma_x(1375) = 2.65 \pm 0.30 \text{ mb}\,. \tag{4.13c}$$

σ_i, the differential cross section at the ith data point, is given in terms of T in (4.11) by

$$\sigma_i = |T(\omega_i)|^2\,. \tag{4.14}$$

The symbol ω_i denotes the four kinematic quantities necessary to describe an event, which we choose to be W_1, W_2, $\cos\theta_n$, and $\cos\phi$, as defined in Fig. 3. The theoretical total cross section σ_T is obtained from the event point cross sections by

$$\sigma_T = \int \sigma_i(\omega) d^4\omega\,. \tag{4.15}$$

In terms of the conventional likelihood function, χ^2 is just $-2\ln L$, where L is the product of the likelihood for $\bar{\sigma}$ around σ_x with error $\Delta\sigma_x$ by the likelihood for N events of values σ_i (with total cross section $\bar{\sigma}$). The quantity $\bar{\sigma}$ is implicitly varied in the analysis (for minimum χ^2). If $\Delta\sigma_x = 0$, then $\bar{\sigma} = \sigma_x$.

This definition of χ^2 allows a direct interpretation of parameter errors which are defined, in the canonical way, as that change in one parameter which causes χ^2 to increase by one after χ^2 has been minimized with respect to all parameters. This definition also allows direct addition of other χ^2 constraints, such as isotopic partial-wave cross sections. When multiple charge channels are used, the corresponding χ^2 values are simply added together.

The algorithm for minimization is a standard one. χ^2 is first expanded to second order in the parameter increments

$$\chi^2 \simeq \chi_0{}^2 + \beta^T \Delta p + \tfrac{1}{2}(\Delta p)^T A \Delta p\,, \tag{4.16}$$

where Δp_k is the change in the kth parameter, β_k is the kth component of gradient $(-\partial\chi^2/\partial p_k)$, and A_{jk} is the second-derivative matrix $A_{jk} = \partial^2\chi^2/\partial p_j \partial p_k$. Here we have used a vector notation where β^T is the transpose of β.

The change, $\Delta p_{\min}$, which minimizes the approximate χ^2 is

$$\Delta p_{\min} = -A^{-1}\beta\,. \tag{4.17}$$

Equations (4.12), (4.16), and (4.17) are iterated numerically until a solution is obtained ($\beta \to 0$) at which point the parameter errors are simply

$$\epsilon_k = (2A^{-1}{}_{kk})^{1/2}\,. \tag{4.18}$$

Problems arise when the algorithm for $\Delta p_{\min}$ results in a χ^2 increase. This normally occurs because of inadequacy of the quadratic approximation or numerical instabilities associated with degeneracies in the parameter space (redundant parameters). We found it efficient and useful to work with the normalized eigenvectors of the real symmetric matrix, A^{-1}.

$$A^{-1} v_j = \lambda_j v_j \,, \qquad v_j^T v_k = \delta_{jk} \,. \tag{4.19}$$

This enables us to express $\Delta p_{\min}$ as a sum of orthogonal changes

$$\Delta p_{\min} = \sum_j \gamma_j v_j \equiv \sum_j \Delta p^j_{\min} \,, \tag{4.20}$$

where

$$\gamma_j = -\lambda_j (\beta^T v_j) \,. \tag{4.21}$$

Since the $\Delta p^j_{\min}$ are an orthogonal set, motion along one of these directions is presumably independent of motion along the other axes.

Although the full second-derivative matrix, A, can be calculated, the search algorithm was found to be more efficient with an approximation developed in the following way. First let us assume that $\Delta\sigma_x = 0$ and that the event points have been binned into equal elements of phase space so that χ^2 can be written

$$\chi^2 = 2N\left(\ln\sigma_x + \frac{\sigma_T}{\sigma_x}\right) - 2\sum_i n_i \ln\sigma_i \,, \tag{4.22}$$

where n_i = number of events in cell i. Then $A_{jk} = \partial^2\chi^2/\partial p_j \partial p_k$ can be written

$$A_{jk} = 2N\frac{\sigma_{T,jk}}{\sigma_x} + 2\sum_i n_i \frac{\sigma_{i,j}\sigma_{i,k}}{\sigma_i^2} - 2\sum_i n_i \frac{\sigma_{i,jk}}{\sigma_i} \,, \tag{4.23}$$

where

$$\sigma_{T,jk} = \frac{\partial^2 \sigma_T}{\partial p_j \partial p_k} \,, \tag{4.24a}$$

$$\sigma_{i,j} = \frac{\partial \sigma_i}{\partial p_j} \,, \tag{4.24b}$$

$$\sigma_{i,jk} = \frac{\partial \sigma_i}{\partial p_j \partial p_k} \,. \tag{4.24c}$$

The last term in this expression is very time-consuming to calculate, but for large numbers the following relations can be used

$$n_i \to N\frac{\omega\sigma_i}{\sigma_T} \,,$$

$$\sigma_T \to \omega \sum_i \sigma_i \,.$$

Therefore, we have

$$\sum_i n_i \frac{\sigma_{i,jk}}{\sigma_i} \to \frac{N\omega}{\sigma_T}\sum_i \sigma_{i,jk} = N\frac{\sigma_{T,jk}}{\sigma_T} \,.$$

This can be used to give the approximate second-derivative matrix

$$A_{jk} \simeq 2N\sigma_{T,jk}\left(\frac{1}{\sigma_x} - \frac{1}{\sigma_T}\right) + 2\sum_i \frac{\sigma_{i,j}\sigma_{i,k}}{\sigma_i^2} \,. \tag{4.25}$$

[Note that in (4.25) we have unbinned the data.] This approximate A is positive-definite as is necessary for a stable minimizing algorithm.

E. Elastic-production-phase (EPP) approximation

A possibly useful method for reducing the number of parameters required to codify the data is to constrain the production amplitudes using information about the (known) elastic partial waves. We will do this using a K-matrix formulation, although other formalisms would undoubtedly suffice and render similar results. The coupled-channel, dimensionless, T matrix is expressed in terms of a K matrix though

$$T = K(1 - iK)^{-1} \,, \tag{4.26}$$

and we write

$$K = \zeta^{1/2} \overline{K} \zeta^{1/2} \,. \tag{4.27}$$

ζ is a diagonal phase-space matrix and $\overline{K}$ is a real-symmetric (in the physical region), reduced K matrix. Note that an element of $\overline{K}$ is expected to be constant at a threshold. It is convenient to split the K matrix into elastic and inelastic components as

$$K = \begin{pmatrix} K_e & K_0^T \\ K_0 & K_i \end{pmatrix} \,. \tag{4.28}$$

The dimensionality of K_i depends upon the number of inelastic channels. An element of K_i represents inelastic-inelastic scattering. K_0 is a vector representing coupling between the elastic channel and the inelastic channels. The equation for T can now be solved to yield

$$T_e = \left(\frac{K'}{1 - iK'}\right)_{ee} = \text{elastic amplitude} \,, \tag{4.29}$$

$$K' = K_e + iK_0^T(1 - iK_i)^{-1}K_0 \,, \tag{4.30}$$

and

$$T_0 = (1 - iK_i)^{-1}K_0(1 + iT_e) = \text{vector of production amplitudes} \,. \tag{4.31}$$

A number of situations could exist for which the matrix $(1 - iK_i)^{-1}$ is essentially real. In these cases the phases of all production amplitudes are equal to the phase of $(1 + iT_e)$:

$$\phi_p = \tan^{-1}\left(\frac{\mathrm{Re}(T_e)}{1 - \mathrm{Im}(T_e)}\right) \,. \tag{4.32}$$

We refer to ϕ_p as the elastic production phase (EPP). For open inelastic channels $K_0 = \zeta_e^{1/2}\overline{K}_{ei}\zeta_i^{1/2}$ is real but may be either positive or negative, which implies that the EPP for a given production amplitude is known modulo π.

A region where EPP seems reasonable is where

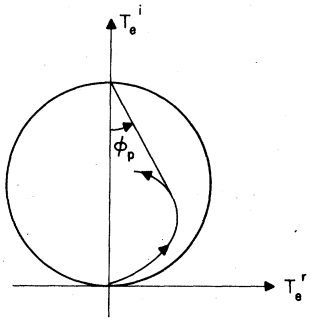

FIG. 9. Argand diagram for an elastic reaction showing the elastic production phase angle ϕ_p.

the inelastic channels are just opening ($\zeta_i \sim 0$; hence, $K_i \sim 0$). In this case

$$T_0 \sim K_0(1+iT_e). \tag{4.33}$$

A second situation leading to EPP involves channels that are kinematically closed, giving imaginary phase-space factors, for which $(1-iK_i)^{-1}$ becomes just a real mixing matrix. The graphical interpretation of EPP is shown in Fig. 9 which gives the Argand diagram for an elastic reaction and indicates the angle ϕ_p. One sees that for an elastic resonance such as the Δ, we have $T_e^r \to 0$, and $\phi_p \to 0$. In Appendix C we include a further discussion of some aspects of the EPP approximation.

The elastic production phases used in the present work are given in Table IV. In the following section we present the results of analyses with appropriate production amplitudes constrained to have these phases and analyses in which the phases were freely searched. The latter phases are referred to as SPP or "searched production phases." We feel that the best representation for Δ production waves is obtained by utilizing the EPP constraint. We note that the ϵ production wave $PS11(\epsilon N)$ has a real contribution from the background and that, as discussed further below, the phase of the searched component is large. These facts suggest that the combined (background plus isobar) amplitude has something near the EPP prediction for this wave.

TABLE IV. The elastic production phases (in degrees) used for the EPP solutions.

W (MeV)	P_{11}	P_{33}	D_{13}	D_{33}
1340	22.6	−36.1	3.2	0.0
1360	28.5	−32.2	4.3	0.0
1375	32.0	−29.5	5.5	0.0

F. Results

In our fitting we imposed on the $D33$ production amplitude the requirement that it be real, since the corresponding elastic amplitude has small phase shifts at the energies involved, and we kept the $D13$ phase at the *EPP* value for the *SPP* solution. We tested these assumptions against the data by making random starts with these amplitudes complex and also by allowing the fitting program search to complex values from the real valued solutions. In the second case, no significant improvement in χ^2 was obtained. In the first case the effect was to increase the number of local minima, reached from random starts, with bad values of χ^2—without uncovering any better minima than those found with the reality restriction.

Because of the large value of the $DS13(\pi\Delta)$-$DP13(\epsilon N)$ overlap, the search program exhibited, in some cases, an instability in which it searched to large cancelling values of $A(DS33\text{-}\pi\Delta)$, $A(DS13\text{-}\pi\Delta)$, and $A(DP13\text{-}\epsilon N)$. The meaning of the large overlap is that, to a good approximation, both $DS13(\pi\Delta)$ and $DP13(\epsilon N)$ describe transitions to the same $\pi\pi N$ configuration. However, we expect that the amplitude for making the p-wave ϵN transition should be suppressed relative to that for going to the $\pi\Delta$ s wave. For these reasons we set $A(DP13\text{-}\epsilon N)$ equal to zero. This implies that the $DS13(\pi\Delta)$ amplitude which results from the fitting

TABLE V. The preferred EPP solutions in modulus-phase form. The phase, in radians, is given in parentheses. Sign conventions relating our amplitudes to those of other analyses are given in Sec. VIA. The $PP33(\pi\Delta)$ wave is given in Table VIII.

Wave	1340 ± 10 MeV	1360 ± 10 MeV	1375 ± 5 MeV
$PP11(\pi\Delta)$	0.102 ± 0.007 (0.39)	0.126 ± 0.008 (0.49)	0.179 ± 0.010 (0.56)
$PS11(\epsilon N)$	0.201 ± 0.007 (1.552 ± 0.063)	0.245 ± 0.008 (1.483 ± 0.068)	0.235 ± 0.009 (1.362)
$DS13(\pi\Delta)$	0.067 ± 0.007 (0.055)	0.096 ± 0.007 (0.075)	0.109 ± 0.007 (0.096)
$DS33(\pi\Delta)$	0.04 ± 0.013 (0)	0.084 ± 0.015 (0)	0.083 ± 0.014 (0)
χ^2	−8.0	74.0	9.0

TABLE VI. The SPP solutions in modulus-phase form. The phase, in radians, is given in parentheses. Sign conventions relating our amplitudes to those of other analyses are discussed in Sec. VIA. The $PP33(\pi\Delta)$ wave is given in Table VIII.

Wave	1340 ± 10 MeV	1360 ± 10 MeV	1375 ± 5 MeV
$PP11(\pi\Delta)$	0.084 ± 0.007	0.114 ± 0.009	0.162 ± 0.010
	(1.123 ± 0.110)	(0.96 ± 0.12)	(0.975 ± 0.090)
$PS11(\epsilon N)$	0.182 ± 0.007	0.237 ± 0.008)	0.238 ± 0.009
	(1.444 ± 0.071)	(1.471 ± 0.068)	(1.412 ± 0.073)
$DS13(\pi\Delta)$	0.055 ± 0.006	0.088 ± 0.009	0.090 ± 0.009
	(0.055)	(0.075)	(0.096)
$DS33(\pi\Delta)$	0.057 ± 0.012	0.093 ± 0.015	0.107 ± 0.016
	(0)	(0)	(0)
χ^2	−30.0	64.0	−4.8

has a small part representing $DP13(\epsilon N)$ production.

With the above restrictions on the production amplitudes, we obtained the following results from the maximum-likelihood analysis.

1. Preferred solutions

The preferred solutions from our analysis are presented in Tables V and VI in modulus-phase form; with the phase in radians. The Table V (EPP) solutions were obtained by keeping the Δ phases fixed at the elastic production values given in Table IV. Table VI (the SPP solutions) involved a searching of the $PP11(\pi\Delta)$ phase. This generally resulted in χ^2 reductions of between 10 and 20, a small reduction in the magnitude of most Δ production waves, and a uniform increase in the ratio of $DS33$ to $DS13$ Δ production.

2. Alternative solutions

The preferred solutions were obtained from hundreds of random starts at each of the three energies. Generally, the preferred values were distinguished by substantially lower χ^2's than those alternative solutions which were discovered with this procedure. An exception occurred at 1340 MeV where the alternative EPP solution given in Table VII actually had a somewhat lesser χ^2 (−14.4 vs −8), but was of a clearly different character than the preferred solutions. When the $PP11(\pi\Delta)$ phase was released, the alternative solution searched to the SPP 1340 value given in Table VI. Attempts to duplicate this solution at 1360 and 1375 MeV were not successful, so we view it as an artifact of the 1340 data and not as a viable, stable solution.

3. PP33(πΔ) solution

For those random starts which included searching of the $PP33(\pi\Delta)$ wave, this amplitude invariably searched to quite a small number and the resultant solutions were basically those listed in Tables V, VI, and VII. In order to determine more precisely the $PP33(\pi\Delta)$ amplitude we resorted to a one-dimensional χ^2 mapping in which we fixed the amplitudes at their EPP (Table V) values, fixed the phase of $PP33(\pi\Delta)$ at its predicted elastic value, and then varied the modulus of the amplitude thereby producing a sharply minimized χ^2 curve; the results are indicated in Table VIII. Table VIII also includes results from a similar procedure using the SPP (Table VI) solutions. These results are used, with extrapolation, to evaluate the $\Delta\pi\Delta$ coupling constant in Sec. V.

4. ξ parameter

We used the same methodology for determining the ξ parameter at each of the three energies as was used for determining the $PP33(\pi\Delta)$ amplitude; namely, a χ^2 mapping using the EPP solutions from Table V. Our procedure for determining ξ involved, first, replacing the chiral-symmetry-breaking contribution of Eq. (A12) by the full one-pion-exchange diagram of Aaron *et al.*[29] The former (specifically, the multiplier of ξ) is recaptured

TABLE VII. The alternative EPP 1340 solution discussed in Sec. IV F in modulus-phase form. The phase, in radians, is given in parentheses.

Wave	1340 ± 10 MeV
$PP11(\pi\Delta)$	0.092 ± 0.007
	(0.39)
$PS11(\epsilon N)$	0.149 ± 0.008
	(0.66 ± 0.14)
$DS13(\pi\Delta)$	0.065 ± 0.005
	(0.055)
$DS33(\pi\Delta)$	0.004 ± 0.008
	(0)
χ^2	−14.4

TABLE VIII. The $PP33(\pi\Delta)$ solution as discussed in Sec. IV F in modulus-phase form. The phase, in radians, is given in parentheses.

Wave	1340 ± 10 MeV	1360 ± 10 MeV	1375 ± 5 MeV
	$PP33(\pi\Delta)$ amplitude (from EPP solution)		
$PP33(\pi\Delta)$	−0.004 ± 0.020	0.055 ± 0.013	0.030 ± 0.016
	(−0.65)	(−0.56)	(−0.50)
χ^2	−9.6	69.0	7.8
	$PP33(\pi\Delta)$ amplitude (from SPP solution)		
$PP33(\pi\Delta)$	−0.047 ± 0.012	−0.091 ± 0.013	−0.084 ± 0.010
	(−0.65)	(−0.56)	(−0.50)
χ^2	−33.0	59.6	−6.6

from the latter by multiplying by

$$R^{-1} = -\frac{3}{16\pi}\frac{m_\pi^2}{f_\pi^2}(W_{\pi\pi}e^{i\delta_{\pi\pi}}\sin\delta_{\pi\pi}/q_{\pi\pi})^{-1}. \quad (4.34)$$

The results for the coefficient of the one-pion-exchange diagram, let us call it $\tilde{\xi}$, are (for one particular set of starting points):

$$\tilde{\xi}(1340\text{ MeV}) = -0.06 \pm 0.30, \quad (4.35a)$$

$$\tilde{\xi}(1360\text{ MeV}) = +0.60 \pm 0.50, \quad (4.35b)$$

$$\tilde{\xi}(1375\text{ MeV}) = -0.30 \pm 0.30. \quad (4.35c)$$

These give, when averaged, $\tilde{\xi} \approx 0.08 \pm 0.40$; the values of $\tilde{\xi}$ were obtained from the mapping procedure described above in Sec. III. They are sensitive to the starting values; the errors, we believe, are realistic ones.

To find the value of the conventional ξ we need to multiply $\tilde{\xi}$ by the factor R. We have evaluated R in three ways: (a) taking the limit $W_{\pi\pi} \to 2m_\pi$ and using the $\xi = 0$ $\pi\pi$ scattering lengths; (b) taking the limit $W_{\pi\pi} \to 2m_\pi$ and using the $\xi = -2$ $\pi\pi$ scattering lengths; and (c) averaging over the Dalitz plot. The results for R, in these three cases, are

$$R_a = -\tfrac{7}{3}, \quad (4.36a)$$

$$R_c \approx R_b = -4. \quad (4.36b)$$

These give

$$\xi_a = -0.2 \pm 0.9, \quad (4.37a)$$

$$\xi_{b,c} = -0.3 \pm 1.6. \quad (4.37b)$$

ξ is thus consistent with zero, although we cannot rule out, on the basis of the present data, the value $\xi = -2$. The reader should recall that our method for determining ξ is essentially to ask for the deviation of the amount of $SP11(\epsilon N)$ production from the amount predicted by chiral symmetry. Because of the small size of the $SP11(\epsilon N)$ one-pion-exchange cross section,[29] the extraction of ξ requires some delicacy.

5. *Other charge states*

Using the above results for the isobar model amplitudes and the expressions of Appendix A for the chiral-symmetry-background amplitudes, we may calculate the cross sections for all possible charge state processes with a proton target. The results are given in Table II. Comparing these results to the chiral-symmetry contribution of Fig. 7, we see that the large percentage of ϵN production in $\pi^+\pi^-n$ implies that production of non-zero-charge dipion states should be significantly closer to the current-algebra predictions than is the production of zero-charge states, to which ϵN production contributes.

V. $\Delta\pi\Delta$ COUPLING CONSTANT

In this section we use the results of the isobar analysis to determine the value of the $\Delta\pi\Delta$ coupling constant. Our method is first to use the $PP33(\pi\Delta)$ production amplitudes to compute the total cross section for this channel from the relation

$$\sigma = \frac{4\pi}{p^2}(J+\tfrac{1}{2})C_I^{\,2}|A|^2, \quad (5.1)$$

where p is the c.m. momentum of the initial state, C_I is the product of the relevant isospin Clebsch-Gordan coefficients, and A is either the SPP or EPP amplitude from Table VIII. We then compare (5.1) with the same total cross section calculated from the Feynman diagram of Fig. 10. This diagram involves the $\pi N\Delta$ coupling constant, which we can fix from the Δ width, and the $\Delta\pi\Delta$ coupling constant. The "experimental" values of A will thus give a direct determination of the $\Delta\pi\Delta$ coupling.

In order to evaluate the diagram of Fig. 10 we must overcome two difficulties that are present in the field theory of a spin-$\frac{3}{2}$ particle. First, no completely consistent method of quantization is

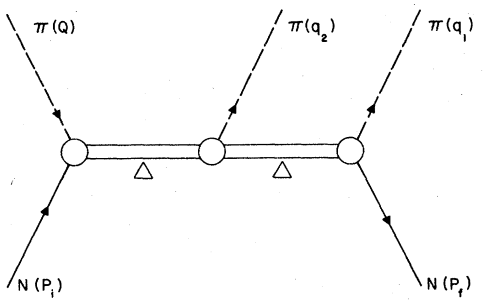

FIG. 10. The Feynman diagram for $PP33(\pi\Delta)$ production.

available; some anticommutators are necessarily incompatible with a positive definite metric.[35,36] We shall not let this stop us from doing phenomenology but shall endeavor to be as consistent as possible. Second, the off-mass-shell couplings and the propagator involve extra parameters, one of which is free and can be chosen for convenience and others whose values are chosen to fit a consistency criterion. Denoting the spin-$\frac{3}{2}$ field by the 16-component Rarita-Schwinger[37] vector spinor ψ^α, we write the Lagrangian for a spin-$\frac{3}{2}$ particle with no interactions as[36]

$$\mathcal{L} = \tfrac{1}{4}\bar{\psi}^\alpha[g_{\alpha\beta}\gamma^\mu + \mathfrak{W}(\delta^\mu_\alpha\gamma_\beta + \delta^\mu_\beta\gamma_\alpha) - \tfrac{1}{2}(3\mathfrak{W}^2 + 2\mathfrak{W} + 1)\gamma_\alpha\gamma^\mu\gamma_\beta]\partial_\mu\psi^\beta + \text{H.c.} + \tfrac{1}{2}m_\Delta\bar{\psi}^\alpha[g_{\alpha\beta} - (3\mathfrak{W}^2 + 3\mathfrak{W} + 1)\gamma_\alpha\gamma_\beta]\psi^\beta , \quad (5.2)$$

where we use the metric and γ conventions of Bjorken and Drell.[38] No physical result can depend on the value of the parameter $\mathfrak{W}$, which may be chosen arbitrarily. The spin-$\frac{3}{2}$ propagator also involves $\mathfrak{W}$ and takes the form

$$S^{\alpha\beta}(p) = [p^2 - (m_\Delta - \tfrac{1}{2}i\Gamma_\Delta)^2]^{-1}\left\{(\not{p} + m_\Delta)\left[-g^{\alpha\beta} + \tfrac{1}{3}\gamma^\alpha\gamma^\beta + \frac{1}{3m_\Delta}(\gamma^\alpha p^\beta - \gamma^\beta p^\alpha) + \frac{2}{3m_\Delta^2}p^\alpha p^\beta\right]\right.$$
$$\left. -(p^2 - m_\Delta^2)\frac{1}{3m_\Delta^2}\left(\frac{\mathfrak{W}+1}{2\mathfrak{W}+1}\right)\left[\left(\frac{\mathfrak{W}+1}{4\mathfrak{W}+2}\not{p} - \frac{\mathfrak{W}}{2\mathfrak{W}+1}m_\Delta\right)\gamma^\alpha\gamma^\beta + \gamma^\alpha p^\beta + \frac{\mathfrak{W}}{2\mathfrak{W}+1}\gamma^\beta p^\alpha\right]\right\}. \quad (5.3)$$

Since the form of the propagator simplifies considerably with $\mathfrak{W} = -1$, we shall use this value in our calculations.

As noted above, the interaction terms of the Lagrangian involving spin-$\frac{3}{2}$ particles contain additional parameters. The $\pi N\Delta$ vertex, for example, is given by

$$g_{\pi N\Delta}\bar{\psi}(g_{\alpha\beta} + \lambda\gamma_\alpha\gamma_\beta)\psi^\beta\partial^\alpha\phi . \quad (5.4)$$

The most general form for λ is

$$\lambda = \tfrac{1}{2}\mathfrak{W}(1 + 4Z) + Z ,$$

where Z is another parameter. This expression was first obtained by Nath, Etemadi, and Kimel[39] who showed that Z is required to be $\frac{1}{2}$. In later work by Hagen[36] it was shown that $Z = \frac{1}{2}$ is required in order to satisfy the Johnson-Sudarshan theorem[35] that the constraint equation continue to exist in the presence of the interaction (5.4). For $\mathfrak{W} = -1$ this condition implies that the time component ψ^0 should not appear in the field equation that results from varying $\bar{\psi}^0$. Thus the expense of eliminating the final terms in (5.3) by choosing $\mathfrak{W} = -1$ is to have $\lambda = -1$ and additional terms in (5.4).

In our work we have replaced the resonance denominator of Eq. (5.3) with the isobar propagator of Woloshyn, Moniz, and Aaron[40]:

$$D(s) = s - m_r^2 + \frac{1}{3}\int_0^\infty \frac{dk}{(2\pi)^2}\frac{\omega_k + E_k}{\omega_k E_k}\frac{k^4 v(k^2)}{(\omega_k + E_k)^2 - s} .$$

The form factor

$$v(k^2) = \frac{g}{k^2 + \beta^2} ,$$

and $m_r = 6.83$ fm^{-1}, $\beta = 1.8$ fm^{-1}, and $g = 3.14 m_\Delta^2$. This expression has been shown to fit the 3-3 partial-wave phase shift for πN scattering with a χ^2 which is as low as other three-parameter fits, and it has a substantial theoretical foundation. The values of the $\Delta\pi\Delta$ coupling constant are sensitive only to the imaginary part of the resonance denominator; we tried a number of other forms of the parametrization of the propagator with the result that the values of $g_{\Delta\pi\Delta}$ could be substantially increased over those quoted below only with a width of the form $\Gamma_0(q/q_0)^3$. Such expressions, however, give very bad fits to the πN scattering phase shifts.

The coupling constant in (5.4) is related to the decay width by

$$g_{\pi N\Delta}^2 = 192\pi\Gamma_\Delta \frac{m_\Delta^5}{F^3(m_\Delta^2, m^2, m_\pi^2)[(m + m_\Delta)^2 - m_\pi^2]} , \quad (5.5)$$

where

$$F(a,b,c) \equiv [a^2 + b^2 + c^2 - 2ab - 2ac - 2bc]^{1/2} ,$$

and m_Δ, m, and m_π are the Δ, N, and π masses, respectively. Using $\Gamma_\Delta = 0.110$ GeV gives the $g_{\pi^+ p\Delta^{++}}$ coupling. The coupling constant for other

charge states is obtained from this value using appropriate $C-G$ coefficients. We note that, in our opinion, the appropriate Δ mass to use in (5.5) is the real part of the position of the pole of the Δ propagator (~1211 MeV), rather than the resonance position (~1236 MeV). In our numerical work we have used both masses; we find that the resulting values of the $\Delta\pi\Delta$ coupling constant differ significantly.

Consider now the $\Delta\pi\Delta$ vertex. Here again there are extra terms with extra parameters. For a pseudoscalar-type coupling we have

$$g_{\Delta\pi\Delta}\bar{\psi}^{\alpha}\gamma_5[g_{\alpha\beta}-\gamma_\alpha\gamma_\beta(A\mathfrak{W}^2+A\mathfrak{W}+\tfrac{1}{4}A+\tfrac{1}{4})]\psi^{\beta}\phi\,. \quad (5.6)$$

This choice of coupling is, of course, not unique. The alternative axial-vector-type coupling is considered below. The consistency criteria[35,36] fix the parameter A to be 3. The reader may note that for $\mathfrak{W}=-1$ and $A=3$, ψ^0 does not appear in the $\delta\bar{\psi}^0$ field equation. Again, there is an extra, off-mass-shell term in the vertex, if we choose $\mathfrak{W}=-1$.

From (5.3), (5.4), and (5.6), the matrix element for the diagram we are considering is given by

$$g_{\Delta^+\pi^-\Delta^0}g_{\pi^+n\Delta^+}g_{\pi^-p\Delta^0}q_1^{\alpha}Q^{\mu}\bar{u}(p_f)(g_{\alpha\beta}-\gamma_\alpha\gamma_\beta)$$
$$\times S^{\beta\rho}(p_f+q_1)\gamma_5[g_{\rho\nu}-\gamma_\rho\gamma_\nu]S^{\nu\sigma}(p_i+Q)[g_{\sigma\mu}-\gamma_\sigma\gamma_\mu]u(p_i)\,, \quad (5.7)$$

where the momentum labels are the same as in Appendix A. There are a large number of terms involved in squaring the eighty term sum in Eq. (5.7) and summing over all spins, but we have managed to calculate the total cross section exactly by using the computer code SCHOONSCHIP.[41]

We define a $\Delta\pi\Delta$ coupling constant, g, by factoring out the Clebsch-Gordan (CG) coefficient

$$g_{\Delta^0\pi^-\Delta^+}{}^2=[C(\tfrac{3}{2}1\tfrac{3}{2};\tfrac{1}{2},-1,\tfrac{3}{2})]^2g^2\,. \quad (5.8)$$

When we compare our cross section with Eq. (5.1), this CG coefficient, and those which must multiply the coupling constant given by (5.5) to get $g_{\pi^+n\Delta^+}{}^2$ and $g_{\pi^-p\Delta^0}{}^2$, will cancel the $C_I{}^2$ factor in (5.1). Using (5.1), we then get an equation for g^2 of the form,

$$\frac{g^2}{4\pi}=C|A|^2\,. \quad (5.9)$$

A is the experimental number for the $PP33(\pi\Delta)$ amplitude as given in Table VIII; C is the result of the calculation of this section. Table IX gives the values of C and $g^2/4\pi$ for the various energies, for two values of m_Δ and for the two solutions for A.

In addition to the pseudoscalar coupling of (5.6) one can equally well consider a $\Delta\pi\Delta$ coupling of the axial-vector form, i.e.,

$$\frac{g_{\Delta\pi\Delta}}{2m_\Delta}\bar{\psi}^{\alpha}\gamma_5\{g_{\alpha\beta}\gamma^{\mu}+[B\mathfrak{W}+\tfrac{1}{2}(B-1)](g^{\mu}_{\alpha}\gamma_\beta+g^{\mu}_{\beta}\gamma_\alpha)+[(\tfrac{1}{2}B+D)\mathfrak{W}^2+D\mathfrak{W}+\tfrac{1}{4}D-\tfrac{1}{8}B+\tfrac{3}{8}]\gamma_\alpha\gamma^{\mu}\gamma_\beta\}\psi^{\beta}\partial_\mu\phi\,. \quad (5.10)$$

TABLE IX. The $\Delta\pi\Delta$ coupling constant as determined for various combinations of the Δ mass, isobar-analysis solutions, and pseudoscalar (P) versus axial-vector (A) interactions.

W	M_Δ	Coupling	$10^{-3}\,C$	$g^2/4\pi$ (SPP)	$g^2/4\pi$ (EPP)
1340 MeV	1211 MeV	P	9.32	$19.7^{+11.6}_{-9.0}$	$0.1^{+5.2}_{-0.1}$
1360	1211	P	4.31	$35.7^{+10.9}_{-9.5}$	$13.0^{+6.9}_{-5.4}$
1375	1211	P	2.54	$17.9^{+8.0}_{-6.5}$	$2.3^{+3.1}_{-1.8}$
1340	1236	P	16.90	$35.7^{+21.1}_{-16.2}$	$0.3^{+9.4}_{-0.3}$
1360	1236	P	7.75	$64.1^{+19.6}_{-17.0}$	$23.4^{+12.4}_{-9.8}$
1375	1236	P	4.58	$32.3^{+14.4}_{-11.8}$	$4.1^{+5.6}_{-3.2}$
1340	1211	A	11.10	$23.4^{+13.8}_{-10.6}$	$0.2^{+6.2}_{-0.2}$
1360	1211	A	4.78	$39.6^{+12.1}_{-10.5}$	$14.5^{+7.6}_{-6.0}$
1375	1211	A	2.71	$19.1^{+8.5}_{-7.0}$	$2.4^{+3.3}_{-1.9}$
1340	1236	A	21.00	$44.4^{+26.2}_{-20.1}$	$0.3^{+11.7}_{-0.3}$
1360	1236	A	9.00	$74.6^{+22.8}_{-19.8}$	$27.2^{+14.4}_{-11.4}$
1375	1236	A	5.11	$36.0^{+16.1}_{-13.1}$	$4.6^{+6.2}_{-3.6}$

When the Δ is on the mass shell, this coupling is identical to the one in (5.6). Consistency of the constraint equations fixes the various parameters, in this case to $B=D=1$. It is useful to notice that, for these values, (5.10) reduces to

$$\frac{g_{\Delta\pi\Delta}}{2m_\Delta} i\epsilon_{\alpha\beta\mu\rho}\bar{\psi}^\alpha \gamma^\rho \psi^\beta \partial^\mu \phi \,. \tag{5.10a}$$

Using this coupling we can again calculate C from Eq. (5.9); the results are given in the bottom half of Table IX.

Since the values of the coupling g given in Table IX correspond to the definition (5.8), they must be multiplied by a CG coefficient to find the coupling for the particular charge state of interest. As seen from the table, g depends slightly on whether (5.6) or (5.10) is used, with the axial-vector coupling values being slightly larger. The value chosen for the mass of the Δ, however, has a much stronger effect on the result for g. A value slightly above the resonance position, $m_\Delta = 1236$ MeV, gives values for $g^2/4\pi$ twice as large as those obtained if m_Δ is taken as the real part of the pole position, $m_\Delta = 1211$ MeV. This is almost entirely due to the difference in $g_{\pi N\Delta}$ as calculated from (5.5).

What value does theory predict for g? From the pion-nucleon coupling, SU(6) gives the $\Delta^{++} \to \Delta^{++}\pi^0$ axial-vector coupling constant[42]

$$\frac{g_{\Delta^{++}\pi^0\Delta^{++}}{}^2}{4\pi} = 9\,\frac{G^2}{4\pi}\left(\frac{2\bar{M}_{10}}{\mu_{00}}\right)^2 \simeq 77 \,. \tag{5.11}$$

Here $G^2/4\pi = \frac{1}{2}$, μ_{00} is the average mass of the meson octet, 700 MeV, and $\bar{M}_{10}$ is the average mass of the baryon decuplet, 1450 MeV. The predicted value for the g^2 of Eq. (5.9) is thus

$$\frac{g^2}{4\pi} = [C(\tfrac{3}{2}1\tfrac{3}{2};\tfrac{3}{2}0\tfrac{3}{2})]^{-2}\,\frac{g_{\Delta^{++}\pi^0\Delta^{++}}{}^2}{4\pi} \cong 130 \,. \tag{5.12}$$

The $\Delta\pi\Delta$ coupling constant has also been treated in U(12); the resulting value is in close agreement with the SU(6) answer.[43]

We can also make a theoretical prediction of g by extending the Goldberger-Treiman[44] relation to spin-$\frac{3}{2}$ particles (see Appendix D),

$$g_{\pi^a \Delta^b} = \sqrt{2}\, m_\Delta (g_A)_{\Delta^a\Delta^b}/f_\pi \,. \tag{5.13}$$

$(g_A)_{\Delta^a\Delta^b}$ is the axial-vector coupling constant for the semileptonic decay $\Delta^a \to \Delta^b e\bar{\nu}$. This is unknown but can be calculated with some confidence in a model, such as the MIT bag model, where the nucleon g_A is predicted accurately.[45] In the bag model, one finds

$$(g_A)_{\Delta^+\Delta^0} = 1.30 \,, \tag{5.14a}$$

$$(g_A)_{\Delta^{++}\Delta^+} = 1.13 \,. \tag{5.14b}$$

Usually, in using the Goldberger-Treiman (GT) relation f_π is fixed to give 14.6 for $g_{pp\pi^0}{}^2/4\pi$. Thus we have $f_\pi = 0.622 m_\pi$, if we use the experimental value for the nucleon axial-vector coupling, $g_A = 1.25$, or we have $f_\pi = 0.544 m_\pi$, if we use the bag-model prediction of 1.09 for g_A. In these two cases we get

$$\frac{g^2}{4\pi} = 102 \text{ or } 133 \tag{5.15}$$

for $m_\Delta = 1236$ MeV (100 or 130 if $m_\Delta = 1211$ MeV). These numbers agree fairly closely with the SU(6) result, as expected, since both methods give good values for the nucleon-pion coupling constant.[46]

The startling thing is that, with the possible exception of the solution at $W = 1360$ MeV for $m_\Delta = 1236$ MeV, the theoretical values (5.12) or (5.15) are several times and several standard deviations larger than the experimental values given in Table IX. Further it is hard to see how the A values of Table VIII could be seriously in error since an A equal to, or larger than, 0.1, as required to agree with (5.12) or (5.15), would correspond to a $PP33$ ($\pi\Delta$) isobar contribution of more than 5% of the total cross section. But it also seems that the GT relation should remain true for spin $\frac{3}{2}$. Although there are additional terms in the matrix elements of the axial-vector or pion current from those retained in Eq. (5.13), they vanish as the momentum transfer (pion momentum) goes to zero. The PCAC smoothness assumption therefore implies that these terms should not significantly affect our result for $g_{\Delta\pi\Delta}$. Furthermore, there are theoretical reasons to expect that the appropriate mass to use in our calculations is the real part of the position of the pole of the Δ propagator (~1211 MeV), rather than the resonance position (~1236). Also the restrictions which give the EPP solution for A, rather than the SPP solution, seem very reasonable. Each of these things severely increases the disagreement between theory and experiment.

Finally we note that the preliminary results from the Berkeley–Carnegie-Mellon elastic-phase-shift analysis[47] provide an upper limit for $A(PP33 - \pi\Delta)$ if we make the reasonable assumption that there is no other significant $P33$ production mechanism. Using the values of η and δ at W equal to 1356 or 1394 MeV from this analysis, we find that

$$\begin{aligned} |A| &= 0.02^{+0.05}_{-0.02} \quad (1356 \text{ MeV}) \,, \\ |A| &= 0.01^{+0.07}_{-0.01} \quad (1394 \text{ MeV}) \,. \end{aligned} \tag{5.16}$$

Extrapolating the C values of Table IX to these energies and averaging over the two types of coupling, the two values for m_Δ, and the two different

energies we find

$$\frac{g^2}{4\pi} = 2^{+25}_{-2} . \tag{5.17}$$

The maximum value for $g^2/4\pi$ from the 1-standard-deviation error for any energy, m_Δ value, or coupling type is 52.

The Berkeley–Carnegie-Mellon group also has inelasticities and phase shifts at 1321 MeV, which yield a similar value for $|A|$. We did not include these data because the extrapolation of C could not be done accurately. C would, of course, be larger so that these data would not give as good an upper bound on $g^2/4\pi$ from the 1-standard-deviation error, although the values of $g^2/4\pi$ would still be consistent with zero.

VI. CONCLUSIONS

A. Comparison with Herndon *et al.*

There is one previous partial-wave isobar-model analysis, by a Berkeley-SLAC collaboration,[6] with which our results should be compared. Both analyses use, in principle, the same data set, although the number of events we found on the tapes supplied to us (4000 with energy below 1380 MeV) does not correspond to the number (5200 with energy below 1380 MeV) reported in Table III of Ref. 6.

We reproduce in Table X the results of Herndon *et al.*[6] for isobar production at 1310, 1340, and 1370 MeV. We recall that our results for the amplitudes for ϵN production are only approximately comparable with those of Ref. 6 since we include a chiral-symmetric background separately. To carry out the comparison we must consider the question of sign conventions which was mentioned briefly in Sec. IV. In order to compare the results of isobar analyses with the predictions of various models of strong interactions, it has been generally agreed to adopt the following *standard conventions* in constructing the isobar expansions [i.e., Eqs. (4.3) and (4.4)]:

(i) The baryon should appear first in all Clebsch-Gordan coefficients (CGC's).

(ii) The particle-isobar orbital angular momentum should appear before the channel spin in all CGC's.

(iii) The angle in any Y_{lm} is measured to the first particle in the corresponding isospin CGC.

Neither we nor Herndon *et al.* followed the latter conventions, so below we relate our amplitudes and those of Ref. 6 to those defined by the above *standard conventions*:

$$A_\Delta(\text{present}) = +(-1)^l i A_\Delta(\text{Herndon})\eta$$
$$= +(-1)^{I+1/2+l} i A_\Delta(\text{standard})\eta , \tag{6.1}$$

$$A_\epsilon(\text{present}) = -(-1)^l i A_\epsilon(\text{Herndon})\eta$$
$$= A_\epsilon(\text{standard})\eta . \tag{6.2}$$

Here l_i is the initial orbital angular momentum. The reader is reminded that our incident pion is taken along the $-z$ axis, while that of Herndon *et al.* is along the $+z$ axis. In (6.1) and (6.2) $\eta(=\pm 1)$ defines the overall phase between our amplitudes and those of Ref. 6. An overall minus is irrelevant to Herndon *et al.* This is because the phases of their amplitudes are determined by a partial-wave, coupled-channel, K-matrix calculation from resonant elastic phases. It is not irrelevant to our fit, however, since we determine all isobar production amplitude phases relative to the chiral-symmetry background, which has a phase that is determined by the signs of $g_{\pi NN}$ and f_π. In principle, the sign of the product $g_{\pi NN} f_\pi$ could be determined by an analysis of $\pi^- p \to \pi^- \pi^0 p$ in which the photon exchange amplitude is included along with the chiral-symmetry background. We believe that our isobar amplitudes, as listed in Tables V and VI, have the "correct" overall sign to make them consistent with the sign of the threshold chiral-

TABLE X. The low-energy solutions of Ref. 6. The marginal (–)'s indicate waves with a relative sign change between the definition of our basis functions and those of Ref. 6.

		1310 MeV	1340 MeV	1370 MeV
	$\pi\Delta$ *PP*11	+0.030 + 0.047*i*	+0.048 + 0.075*i*	+0.117 + 0.102*i*
(–)	*DS*13	–0.096 + 0.0052*i*	–0.068 – 0.035*i*	–0.126 – 0.011*i*
(–)	*DD*13	–0.022 + 0.006*i*	–0.020 + 0.002*i*	–0.067 + 0.030*i*
	*PP*31	+0.022 + 0.007*i*	+0.036 + 0.011*i*	+0.066 + 0.0017*i*
(–)	*DS*33	–0.027 – 0.033*i*	–0.038 – 0.047*i*	–0.076 – 0.053*i*
(–)	ρ_3 *DS*13	+0.030 + 0.018*i*	+0.054 + 0.043*i*	+0.102 + 0.043*i*
(–)	ρ_1 *PP*11	–0.0039 + 0.011*i*	–0.0088 + 0.026*i*	–0.0038 + 0.035*i*
(–)	ρ_1 *PP*31	+0.030 + 0.011*i*	+0.045 + 0.016*i*	+0.079 + 0.0049*i*
(–)	ϵN *PS*11	–0.027 – 0.112*i*	–0.037 – 0.130*i*	–0.089 – 0.160*i*
	*SP*11	–0.0041 + 0.017*i*	+0.031 + 0.023*i*	–0.0003 + 0.040*i*
	*DP*13	0.068 + 0.0071*i*	+0.037 + 0.020*i*	+0.086 + 0.0025*i*

symmetry prediction of Olsson and Turner.[11] Thus, we find that $\eta = -1$ in (6.1) and (6.2). In order to facilitate understanding of our conventions, we give numerical results for our amplitudes explicitly in Appendix B.

The comparison between our amplitudes in Tables V and VI and the Herndon *et al.* ones in Table X [corrected by the phases of (6.1) and (6.2) with $\eta = -1$] is rather good. It should be noted that we include ρ production through the antisymmetric part of the chiral-symmetry contribution. ρ production from the isobar amplitude of Herndon *et al.* amounts, at 1340 MeV, to a cross section of about 0.14 mb, neglecting overlaps. In this regard, one should note that Herndon *et al.* use a total experimental cross section of about 1.0 mb, whereas the spectrometer experiment[4] obtains a cross section of 1.35 mb. Our antisymmetric chiral-symmetry $\pi\pi$ cross section is, from Fig. 7, about 0.17 mb; thus the (small) "ρ pieces" agree well.

With regard to the Δ amplitudes, the values of the largest, $PP11$, agree well between the two fits in magnitude and phase. Herndon *et al.* included the nonresonant higher waves $DD13$ and $PP31$ which we omitted while we included the small (but important) resonant $PP33$. The common small waves $DS13$ and $DS33$ agree well. The waves which were not included in both fits amount to a very small percentage of the cross section.

We consider the general agreement in phases between the two fits (with the overall η equal to -1) very important in arguing for the basic validity of both analyses in general and, in particular, for the basic validity of the two very different methods used for determining the phases—coupled-channel K matrices versus interference with the chiral-symmetry background.

B. Corrections to the current-algebra prediction

In Sec. IV we presented the results of our analysis for the chiral-symmetry-breaking parameter. From the deviation of $SP11(\epsilon N)$ production from the chiral-symmetry prediction we concluded that, conservatively, $\xi = -0.3 \pm 1.6$. This result can be checked, and a further comparison with the results of Herndon *et al.*[6] can be made by considering a dispersion relation for the $PS11(\epsilon N)$ amplitude. Our procedure involves estimating the size of the right-hand-cut corrections to $T_{CA} \equiv T_{CS} + \xi T_\xi$ above the three-body threshold at $W_T = 1217$ MeV.

In this section we designate the $PS11(\epsilon N)$ production amplitude $A(W)$. We assume that near the three-body threshold $A(W)$ goes as $q(W - W_T)$, where q is the initial-state c.m. three-momentum. The $(W - W_T)$ factor ensures the $(W - W_T)^2$ production-cross-section behavior. We estimate

TABLE XI. $PS11$ solution of Herndon *et al.*, Ref. 6, expressed in our phase convention [cf. Eq. (6.2)].

W (MeV)	Re$A(PS11)$	Im$A(PS11)$
1310	0.027 18	0.111 73
1340	0.037 13	0.129 87
1370	0.089 27	0.159 83
1400	0.176 21	0.132 71
1440	0.200 80	0.195 31
1470	0.250 13	0.218 94
1490	0.208 44	0.219 47
1520	0.217 49	0.200 63
1540	0.172 37	0.222 57
1650	−0.029 47	0.306 47
1690	−0.052 15	0.147 88
1730	+0.047 47	0.158 61
1770	+0.072 87	0.291 52
1810	−0.115 02	0.323 00
1850	−0.274 36	0.145 30
1890	−0.318 05	0.051 66
1930	−0.295 98	−0.152 28
1970	−0.180 03	−0.256 02

the correction to T_{CA} by assuming that as $W \to W_T$, $A(W)$ goes to A_{CA}, the $PS11$ projection of T_{CA}, and by using this assumption to make a subtraction in a dispersion relation for $A(W)$. Thus,

$$\frac{A(W)}{q(W-W_T)} \cong \left(\frac{A_{CA}}{q(W-W_T)}\right)_{W\to W_T} + \frac{W-W_T}{\pi} \times \int_{m+m_\pi}^{\infty} \frac{\mathrm{Disc}[A(W')/q'(W'-W_T)]}{(W'-W)(W'-W_T)}\, dW' . \tag{6.3}$$

For the purposes of a rough estimate we break the integral (6.3) into two parts, (I) $W \geq 1310$ MeV, and (II) $W < 1310$ MeV. In region I we evaluate the imaginary part of $A(W)$ using the $PS11$ solution of Herndon *et al.*[6] given in our Table XI. In region II we set the lower limit of the integral in (6.3) at W_T (rather than $m + m_\pi$) and proceed as follows:

1. Assume that the Watson phase theorem[48] applies, so we may write

$$\mathrm{Disc}A(W) = e^{i\delta_R(W)} \sin\delta_R(W)\, A(W) . \tag{6.4}$$

In this equation δ_R is the $P11$ elastic πN phase shift. We have used the subscript R to emphasize a fact evident from Tables V and VI; namely, that the tail of the broad Roper resonance at ~1470 MeV contributes to π production, even at very low energies.

2. For δ_R we use the empirical, analytic expression

$$\tan\delta_R(W) \simeq \delta_R(W) = \left(\frac{W-W_T}{1310-W_T}\right)^2 \delta(1310) . \tag{6.5}$$

This gives results fairly close to the analysis of

Ref. 30, where $\delta_R(W)$ varies from about 1.5° to 15° as W goes from 1210 to 1310 MeV. Equations (6.4) and (6.5) together with our original assumption about the threshold behavior of $A(W)$ yields

$$\mathrm{Disc}A(W) = \mathrm{Im}A(1310)\frac{q(W)}{q(1310)}\left(\frac{W-W_T}{1310-W_T}\right)^3. \tag{6.6}$$

Substituting (6.6) into (6.3) and setting $W=W_T$ in the integral gives the dispersive correction δA (from region II) to the current-algebra prediction for A,

$$\delta A \cong \frac{1}{\pi}\frac{q(W)}{q(1310)}\left(\frac{W-W_T}{1310-W_T}\right)^2 \mathrm{Im}A(1310). \tag{6.7}$$

By using Watson's theorem at a higher energy than it is valid [after all, the phase of $A(W)$ at 1310 MeV is approximately 90° and not the 15° of (6.5)] we have underestimated the size of δA.

The phenomenological contribution to (6.3) from region I is roughly equal to that obtained from region II, so the full δA is about twice that given by (6.7). Using this approximate result, the dispersive correction to the current-algebra cross section for $\pi^-p \to \pi^+\pi^-n$ is

$$\delta^2\sigma = 4\pi\lambda^2|2\delta A|^2(\tfrac{4}{9}) \cong 0.1\left(\frac{W-W_T}{1310-W_T}\right)^4|20\,\mathrm{Im}A(1310)|^2\ \mathrm{mb}. \tag{6.8}$$

The effect of the correction (6.8) on a determination of ξ from total-cross-section measurements can be approximated by comparing $\sigma_{\xi=-2}$, $\sigma_{\xi=0}$, and $[(\sigma_{\xi=0})^{1/2}+(\delta^2\sigma)^{1/2}]^2=\sigma^{\mathrm{corr}}$. We do this in Fig. 11 for two values of $\mathrm{Im}A(1310)$, 0.1 and 0.2 at the ends of what seems its plausible range; for the two different ways of calculating $\sigma_{\xi=-2}$, full diagram and full threshold approximation (including the threshold approximation for the coefficient of ξ); and for energies below 250 MeV pion lab energy ($W-W_T=60$ MeV).

From Fig. 11 one can draw the following conclusions:

(1) A pure current-algebra amplitude with $\xi=-2$ and the coefficient of ξ computed in the threshold approximation gives by itself the entire total cross section and is therefore inconsistent with the data if our estimate of the size of the dispersive-part correction to the current-algebra amplitude is correct.

(2) A pure current-algebra amplitude with $\xi=-2$ and the coefficient of ξ computed without making the threshold approximation would be consistent with the total-cross-section measurement, after adding the dispersive part correction, providing $\mathrm{Im}A(1310)$ is at the low end of its range—around 0.1.[49]

(3) If the above estimate is correct, $\xi=0$ and $A(1310)\simeq 0.15$ are consistent with the cross-section measurements at 229 and 255 MeV.

(4) If the above estimate is correct it will be extraordinarily difficult to determine ξ by total-cross-section measurements unless they can be made in the region below $W-W_T=29$ MeV ($T_{1\mathrm{ab}}=195$ MeV). This is because the interference term between the dispersive correction and the current-algebra term vanishes only like $W-W_T$.

C. Summary

The principal results of this work are:

(1) Low-energy bubble-chamber data (1330–1380 MeV) for $\pi^-p \to \pi^+\pi^-n$ gives an (E_+, z_+) distribution in agreement with the preliminary single-arm-spectrometer data[4] (Sec. II).

(2) Section III presents graphs of the current-algebra predictions for five production cross sections for the full, tree-approximation, phenomenological-Lagrangian amplitude, and for the threshold approximation. Note that these two agree well for $\pi^-p \to \pi^+\pi^-n$ for the chiral-symmetric contribution; and that the two calculations for the chiral-symmetry-breaking term (coefficient of ξ) differ appreciably.[49]

(3) Our isobar-model fits show that the dominant pion-production mechanism below 1380 MeV is production through the tail of the Roper $P11$ resonance (see Tables V and VI).

(4) The small penalty in log-likelihood paid for modeling the $PP11(\pi\Delta)$ production phase through the coupled-channel K-matrix elastic-production-phase approximation supports the validity of this approximation (see Secs. IV E and IV F).

(5) The bubble-chamber data by themselves are consistent with both $\xi=0$ and $\xi=-2$; more events are needed to discriminate between these two possibilities. Our technique of determining ξ from the contribution of the chiral-symmetry-breaking term to nonresonant partial waves appears capable of giving an answer for the value of ξ in spite of the large ϵN production in the tail of the Roper resonance (see Sec. IV F 4). Our value for ξ from the bubble-chamber data is

$$\xi = -0.3 \pm 1.6. \tag{6.9}$$

(6) The large value for the ϵN $PS11$ production cross section and the disagreement between the full and threshold-approximation chiral-symmetry-breaking terms indicate caution in inferring ξ from low-energy total-cross-section measurements.[49] At the energies accessible to Gram *et al.*[4] dispersive corrections to the $PS11(\epsilon N)$ wave are the same magnitude as the difference

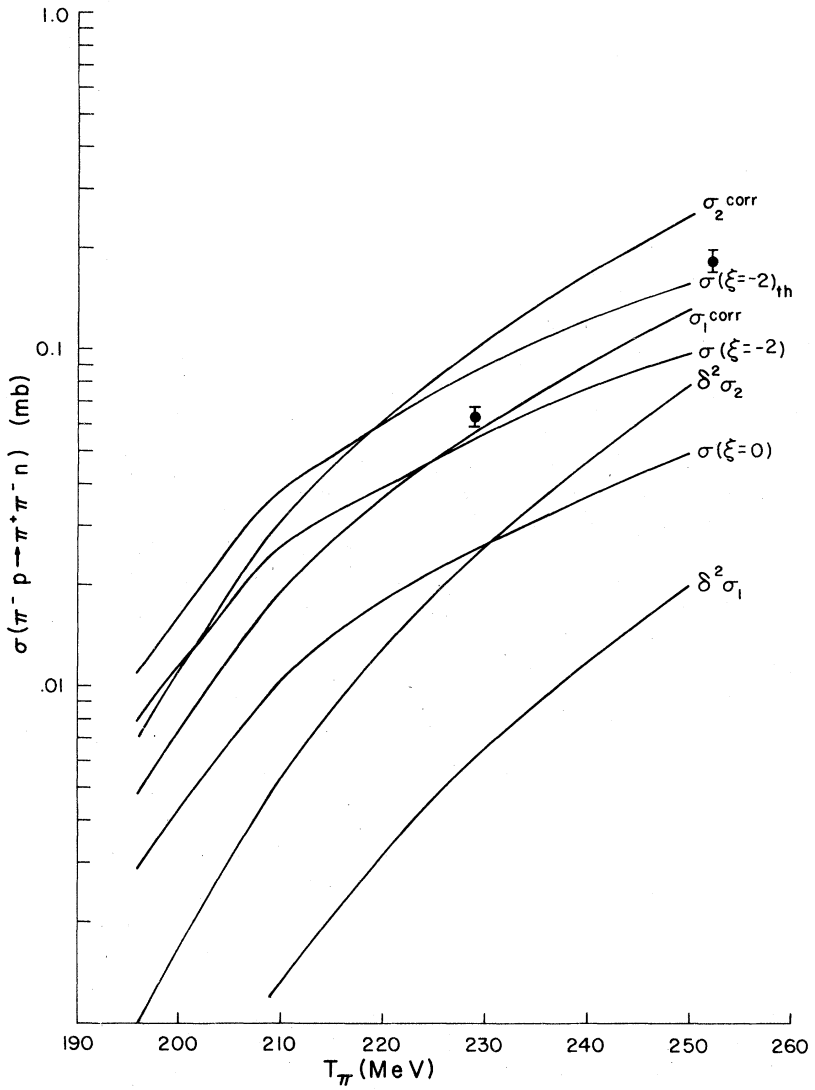

FIG. 11. Cross-section curves in the region $W - W_T = 20 - 60$ MeV, $T_{lab} \simeq 195 - 250$ MeV. $\sigma_i^{corr} = \{[\sigma(\xi=0)]^{1/2} + (\delta^2\sigma_i)^{1/2}\}^2$ where $\mathrm{Im}A(1310) = 0.1,\ 0.2$ for $i = 1, 2$. The two experimental points are the most recent (unpublished) results from the spectrometer experiment, Ref. 4.

between the $\xi = 0$ and $\xi = -2$ amplitudes (see Sec. VI B).

(7) SU(6) and the (generalized to $\Delta\pi\Delta$) Goldberger-Treiman relation both predict a reduced $\Delta\pi\Delta$ coupling constant of approximately $g^2/4\pi \simeq 100$. However, our fits imply (see Sec. V) a considerably smaller value,

$$\frac{g^2}{4\pi} \simeq 40 \pm 20 . \tag{6.10}$$

(8) Our results for the partial-wave isobar amplitudes, on the whole, agree quite well with those of Herndon *et al.*[6] (see Sec. VI A). This agreement is particularly significant in view of the very different methods used for determining the overall phase; our analysis determines the overall sign of the isobar production amplitudes with respect to the well-defined chiral-symmetry-background phase.

(9) From the results of our $\pi^- p \to \pi^+ \pi^- n$ fits we predict in Table II the total cross sections for all other relevant charge states, at 1340, 1360, and 1375 MeV.

In conclusion, we strongly urge the experimental community to produce a more extensive set of *full-kinematics* $\pi\pi N$ data in the low-energy (threshold to 1350 MeV) region for more than one initial and final charge-state choice. We think that the two applications addressed here—determination of the tensor structure of chiral-symmetry breaking (ξ) and determination of $g_{\Delta\pi\Delta}$—by themselves warrant further intensive experimental effort.

ACKNOWLEDGMENTS

It is a pleasure to thank R. Cashmore, L. N. Chang, A. M. Gleeson, B. R. Holstein, D. A. Jenkins, R. Kelly, E. Lomon, G. L. Rebka, R. Rockmore, L. D. Roper, A. Rosenfeld, S. Weinberg, C. N. Yang, and V. S. Zidell for helpful conversations and correspondence. We are indebted to the past collaborators, R. Amado and D. Teplitz, for important contributions to the isobar-model work. One of us (V.L.T.) is grateful to Professor Joseph Sucher for the hospitality of the Institute for Theoretical Physics at the University of Maryland. The work of J.B.C., R.H.H., V.L.T., and R.A. was supported in part by NSF grants to VPI and Northeastern, while the work of D.A.D., Y.G., and R.A.A. was supported in part by DOE contracts with the University of Texas and VPI. The work of R. S. L. was supported by the U. S. Department of Energy under Contract No. EY-76-C-02-0016.

APPENDIX A: PION PRODUCTION AMPLITUDES FROM THE PHENOMENOLOGICAL LAGRANGIAN

We collect here our expressions for the $\pi N \to \pi\pi N$ invariant amplitudes, for all possible charge states, which follow from the Lagrangian of Eqs. (3.8)–(3.11). Our specification of energy-momentum four-vectors is $\pi(Q)+N(p_i)\to\pi(q_1)+\pi(q_2)+N(p_f)$; note that this differs from the notation used in other sections. Our invariant amplitude, T, is released to the S matrix by

$$S_{fi}=i\,\frac{m\,\delta^4(p_f+q_1+q_2-p_i-Q)}{(2\pi)^{7/2}(E_iE_f2\omega_1 2\omega_2 2\omega_Q)^{1/2}}\;T(\pi N\to\pi\pi N)\,. \tag{A1}$$

We follow the conventions and normalizations of Bjorken and Drell.[38] To simplify the expressions for the amplitudes, we define the following:

$$F=\bar u(p_f)\gamma_5 u(p_i)\,, \tag{A2}$$

$$F'(A)=\bar u(p_f)\not{A}\gamma_5 u(p_i)\,, \tag{A3}$$

$$G(A,B)=\bar u(p_f)\not{A}\not{B}\gamma_5 u(p_i)\,, \tag{A4}$$

$$H(A,B,C)=\bar u(p_f)\not{A}\not{B}\not{C}\gamma_5 u(p_i)\,. \tag{A5}$$

We will also need the quantities

$$D_i=(2p_i\cdot Q+m_\pi^2)^{-1}\,, \tag{A6}$$

$$D_f=(2p_f\cdot Q-m_\pi^2)^{-1}\,, \tag{A7}$$

$$D_{1i}=(2p_i\cdot q_1-m_\pi^2)^{-1}\,, \tag{A8}$$

$$D_{1f}=(2p_f\cdot q_1+m_\pi^2)^{-1}\,, \tag{A9}$$

$$D_{2i}=(2p_i\cdot q_2-m_\pi^2)^{-1}\,, \tag{A10}$$

$$D_{2f}=(2p_f\cdot q_2+m_\pi^2)^{-1}\,. \tag{A11}$$

Following Rockmore,[13] we refer to diagrams (a) in Fig. 6 as "one-point" diagrams, (b) as "two-point" diagrams and (c) as a "three-point" diagram. Letting $T^{(i)}$ denote the contribution from the i-point diagram and $T^{(\kappa)}$ the contribution proportional to the nucleon anomalous magnetic moment, we obtain the following expressions for the invariant amplitudes:

(a) $\pi^-(Q)+p(p_i)\to\pi^+(q_1)+\pi^-(q_2)+n(p_f)$

$$T^{(1)}=i\,\frac{g_\pi}{2M}\,\frac{1}{4f_\pi^2}\,\sqrt{2}\,\left[4mF+2F'(q_2)+8mF\,\frac{2Q\cdot q_1-m_\pi^2\xi}{(p_f-p_i)^2-m_\pi^2}\right], \tag{A12}$$

$$T^{(2)}=-i\,\frac{g\pi}{2m}\,\frac{1}{4f_\pi^2}\,\sqrt{2}\,[4mF+6F'(q_2)-2mD_{1f}G(q_1,q_2+Q)-2mD_fG(Q,q_2-q_1)+2mD_{1i}G(q_2+Q,q_1)$$
$$+2mD_iG(q_2-q_1,Q)]\,, \tag{A13}$$

$$T^{(3)}=-i\left(\frac{g_\pi}{2m}\right)^3 2\sqrt{2}\,[2F'(q_2)+2mD_iG(q_2,Q)+2mD_{1i}G(q_2,q_1)-2mD_fG(Q,q_2)-2mD_{1f}G(q_1,q_2)$$
$$-4m^2D_fD_{1i}H(Q,q_2,q_1)-4m^2D_iD_{1f}H(q_1,q_2,Q)]\,, \tag{A14}$$

$$T^{(\kappa)}=-i\,\frac{g_\pi}{2m}\,\frac{\kappa_V}{4f_\pi^2}\,2\sqrt{2}\,[(D_{1f}+D_{1i})(-q_2\cdot Q)F'(q_1)-(D_i+D_f)q_1\cdot q_2\,F'(Q)$$
$$+D_{1f}H(q_1,q_2,Q)+D_fH(Q,q_2,q_1)+D_{1i}H(q_2,Q,q_1)+D_iH(q_2,q_1,Q)]\,. \tag{A15}$$

(b) $\pi^-(Q)+p(p_i)\to\pi^0(q_1)+\pi^0(q_2)+n(p_f)$

$$T^{(1)}=-i\,\frac{g_\pi}{2m}\,\frac{1}{4f_\pi^2}\,\sqrt{2}\,\left[-2F'(Q)-4mF\,\frac{2q_1\cdot q_2+2q_1\cdot Q+2q_2\cdot Q-\xi m_\pi^2}{(Q-q_1-q_2)^2-m_\pi^2}\right], \tag{A16}$$

$$T^{(2)}=-i\,\frac{g_\pi}{2m}\,\frac{1}{4f_\pi^2}\,\sqrt{2}\,[-4mF+6F'(Q)-2mD_{1f}G(q_1,q_2+Q)$$
$$-2mD_{2f}G(q_2,q_1+Q)+2mD_{1i}G(q_2+Q,q_1)+2mD_{2i}G(q_1+Q,q_2)]\,, \tag{A17}$$

$$T^{(3)} = -i\left(\frac{g_\pi}{2m}\right)^3 \sqrt{2}\,[-4mF + 4F'(Q) - 2mD_f G(Q, q_1+q_2) - 2mD_{1f} G(q_1, q_2+Q) - 2mD_{2f} G(q_2, q_1+Q)$$
$$+ 2mD_{2i} G(q_1+Q, q_2) + 2mD_{1i} G(q_2+Q, q_1) + 2mD_i G(q_1+q_2, Q) - 4m^2 D_f D_{2i} H(Q, q_1, q_2)$$
$$- 4m^2 D_f D_{1i} H(Q, q_2, q_1) - 4m^2 D_{1f} D_i H(q_1, q_2, Q)$$
$$- 4m^2 D_{2f} D_i H(q_2, q_1, Q) - 4m^2 D_{1f} D_{2i} H(q_1, Q, q_2) - 4m^2 D_{2f} D_{1i} H(q_2, Q, q_1)], \tag{A18}$$

$$T^{(\kappa)} = -i\,\frac{g_\pi}{2m}\,\frac{\kappa_V}{4f_\pi^2}\,2\sqrt{2}\,[-(D_{1f}+D_{1i})q_2\cdot QF'(q_1) - (D_{2f}+D_{2i})q_1\cdot QF'(q_2)$$
$$+ D_{1f} H(q_1, q_2, Q) + D_{2f} H(q_2, q_1, Q) + D_{1i} H(q_2, Q, q_1) + D_{2i} H(q_1, Q, q_2)]. \tag{A19}$$

(c) $\pi^+(Q) + p(p_i) \to \pi^+(q_1) + \pi^+(q_2) + n(p_f)$

$$T^{(1)} = -i\,\frac{g_\pi}{2m}\,\frac{1}{4f_\pi^2}\,\sqrt{2}\left[2F'(q_1+q_2) + 8mF\,\frac{2q_1\cdot q_2 + \xi m_\pi^2}{(Q-q_1-q_2)^2 - m_\pi^2}\right], \tag{A20}$$

$$T^{(2)} = -i\,\frac{g_\pi}{2m}\,\frac{1}{4f_\pi^2}\,\sqrt{2}\,[-8mF - 6F'(q_1+q_2) + 2mD_{1f} G(q_1, q_2+Q) + 2mD_{2f} G(q_2, q_1+Q)$$
$$- 2mD_{1i} G(q_2+Q, q_1) - 2mD_{2i} G(q_1+Q, q_2)], \tag{A21}$$

$$T^{(3)} = i\left(\frac{g_\pi}{2m}\right)^3 2\sqrt{2}\,[2F'(Q) - 2mD_{1f} G(q_1, Q) + 2mD_{2i} G(Q, q_2) - 2mD_{2f} G(q_2, Q) + 2mD_{1i} G(Q, q_1)$$
$$- 4m^2 D_{1f} D_{2i} H(q_1, Q, q_2) - 4m^2 D_{2f} D_{1i} H(q_2, Q, q_1)], \tag{A22}$$

$$T^{(\kappa)} = i\,\frac{g_\pi}{2m}\,\frac{\kappa_V}{4f_\pi^2}\,2\sqrt{2}[-(D_{1i}+D_{1f})q_2\cdot QF'(q_1) - (D_{2i}+D_{2f})q_1\cdot QF'(q_2) + D_{1f} H(q_1, q_2, Q) + D_{2f} H(q_2, q_1, Q)$$
$$+ D_{1i} H(q_2, Q, q_1) + D_{2i} H(q_1, Q, q_2)]. \tag{A23}$$

(d) $\pi^-(Q) + p(p_i) \to \pi^0(q_1) + \pi^-(q_2) + p(p_f)$

$$T^{(1)} = -i\,\frac{g_\pi}{2m}\,\frac{1}{4f_\pi^2}\left[2F'(q_1) + 8mF\,\frac{q_2\cdot Q - q_1\cdot Q + q_1\cdot q_2 + \frac{1}{2}\xi m_\pi^2}{(Q-q_1-q_2)^2 - m_\pi^2}\right], \tag{A24}$$

$$T^{(2)} = -i\,\frac{g_\pi}{2m}\,\frac{1}{4f_\pi^2}\,[-4mF - 6F'(q_1) + 4mD_{2f} G(q_2, Q+q_1) - 2mD_{1f} G(q_1, Q+q_2)$$
$$+ 4mD_i G(q_2 - q_1, Q) - 2mD_{1i} G(Q+q_2, q_1)], \tag{A25}$$

$$T^{(3)} = -i\left(\frac{g_\pi}{2m}\right)^3 2[-2mF - 2F'(q_1) - 2mD_{1f} G(q_1, q_2) + 2mD_{2f} G(q_2, q_1) + 2mD_{2f} G(q_2, Q)$$
$$+ 2mD_i G(q_2, Q) - 2mD_i G(q_1, Q) - 2mD_{1i} G(Q, q_1) - 4m^2 D_i D_{1f} H(q_1, q_2, Q)$$
$$+ 4m^2 D_i D_{2f} H(q_2, q_1, Q) + 4m^2 D_{2f} D_{1i} H(q_2, Q, q_1)], \tag{A26}$$

$$T^{(\kappa)} = -i\,\frac{g_\pi}{2m}\,\frac{\kappa_V}{4f_\pi^2}\,\frac{1}{m}\,[2(q_2\cdot Q - q_1\cdot Q - q_2\cdot q_1)F + 4mD_{2f} q_1\cdot QF'(q_2) - 2mD_{1f} q_2\cdot QF'(q_1) - 4mD_i q_1\cdot q_2 F'(Q)$$
$$+ 2mD_{1i} q_2\cdot QF'(q_1) + 2G(q_1, Q) - 2G(q_2, Q) + 2G(q_2, q_1) - 4mD_{2f} H(q_2, q_1, Q)$$
$$+ 2mD_{1f} H(q_1, q_2, Q) + 4mD_i H(q_2, q_1, Q) - 2mD_{1i} H(q_2, Q, q_1)]. \tag{A27}$$

(e) $\pi^+(Q) + p(p_i) \to \pi^0(q_1) + \pi^+(q_2) + p(p_f)$

$$T^{(1)} = -i\,\frac{g_\pi}{2m}\,\frac{1}{4f_\pi^2}\left[2F'(q_1) + 8mF\,\frac{Q\cdot(q_2-q_1) + q_1\cdot q_2 + \frac{1}{2}\xi m_\pi^2}{(Q-q_1-q_2)^2 - m_\pi^2}\right], \tag{A28}$$

$$T^{(2)} = -i\,\frac{g_\pi}{2m}\,\frac{1}{4f_\pi^2}\,[-4mF - 6F'(q_1) - 4mD_f G(Q, q_2-q_1) + 2mD_{1f} G(q_1, q_2+Q) - 4mD_{2i} G(q_1+Q, q_2)$$
$$+ 2mD_{1i} G(q_2+Q, q_1)], \tag{A29}$$

$$T^{(3)}=-i\left(\frac{g_\pi}{2m}\right)^3 2[-2mF-2F'(q_1)+2mD_{1f}G(q_1,Q)-2mD_{2i}G(Q,q_2)-2mD_fG(Q,q_2)+2mD_{1i}G(q_2,q_1)$$
$$+2mD_fG(Q,q_1)-2mD_{2i}G(q_1,q_2)+4m^2D_{1f}D_{2i}H(q_1,Q,q_2)-4m^2D_fD_{1i}H(Q,q_2,q_1)$$
$$+4m^2D_fD_{2i}H(Q,q_1,q_2)], \tag{A30}$$

$$T^{(\kappa)}=-i\,\frac{g_\pi}{2m}\,\frac{\kappa_V}{4f_\pi^2}\,\frac{1}{m}\,[2(q_1\cdot q_2+q_1\cdot Q-q_2\cdot Q)F-4mD_fq_1\cdot q_2F'(Q)+2mD_{1f}q_2\cdot QF'(q_1)$$
$$+4mD_{2i}q_1\cdot QF'(q_2)-2mD_{1i}q_2\cdot QF'(q_1)-2G(q_2,q_1)+2G(q_2,Q)-2G(q_1,Q)$$
$$+4mD_fH(Q,q_2,q_1)-2mD_{1f}H(q_1,q_2,Q)-4mD_{2i}H(q_1,Q,q_2)+2mD_{1i}H(q_2,Q,q_1)]. \tag{A31}$$

APPENDIX B: AN EXAMPLE OF THE NUMERICAL RESULTS FOR OUR AMPLITUDES

We give here explicit numerical results for our amplitudes for one bubble-chamber event in order to allow a detailed check of our conventions and our results. We choose an event at approximately 1360 MeV given by

$$\begin{aligned}&\sqrt{s_1}=1099\text{ MeV},\\&\sqrt{s_2}=1199\text{ MeV},\\&z_n=-0.4935,\\&\cos\phi=0.1055,\end{aligned} \tag{B1}$$

where the kinematic variables are defined in Fig. 3. From these values we reconstruct the four-momenta of the initial two and final three particles to be (in MeV)

$$\begin{aligned}&p(\text{initial proton})=(0,0,335,997),\\&p(\text{initial }\pi^-)=(0,0,-335,363),\\&p_1=p(\pi^+)=(-164,73,84,242),\\&p_2=p(\pi^-)=(-6,-73,12,158),\\&p_3=p(n)=(170,0,-96,959).\end{aligned} \tag{B2}$$

Note our convention of having the initial nucleon along the $+\hat{z}$ axis. In Tables XII and XIII we give our results for the basis functions of Eqs. (4.3) and (4.4), respectively, for $\mu_f=\mp\frac{1}{2}$ and $\mu_i=+\frac{1}{2}$. The phase-space factor is adjusted such that each of these basis functions satisfies

TABLE XII. Our results for the ϵN basis function of Eq. (4.3).

Wave	$10^3\,X_\epsilon(\mu_i=\frac{1}{2},\ \mu_f=-\frac{1}{2})$	$10^3\,X_\epsilon(\mu_i=\frac{1}{2},\ \mu_f=\frac{1}{2})$
$PS11$	0	$-2.64-0.717i$
$DP11$	$2.62+0.712i$	$2.98+0.808i$

$$\int|X_\alpha|^2d\rho=a4\pi\chi^2|\text{CG(isospin)}|^2, \tag{B3}$$
$a=2$ for ϵN,
$a=1$ for $\pi\Delta$.

We define amplitudes $A^{(j)}$ related to the chiral-symmetry invariant amplitudes of Appendix A by

$$T^{(j)}_{\rm CS}=iA^{(j)}_{\rm CS}. \tag{B4}$$

$A_{\rm CS}=\sum_jA^{(j)}_{\rm CS}$ in the threshold approximation is the amplitude of Olsson and Turner.[11] We obtain for $A_{\rm CS}$ at our kinematical point

$$\begin{aligned}A_{\rm CS}(p_1,p_2)&=-0.174\times10^{-3}+0.157\times10^{-3}i\quad(\mu_f=-\tfrac{1}{2})\\&=-0.137\times10^{-3}-0.231\times10^{-5}i\quad(\mu_f=+\tfrac{1}{2}).\end{aligned} \tag{B5}$$

If we interchange the pions we obtain

$$\begin{aligned}A_{\rm CS}(p_2,p_1)&=0.991\times10^{-4}-0.240\times10^{-3}i\quad(\mu_f=-\tfrac{1}{2})\\&=-0.774\times10^{-4}+0.106\times10^{-4}i\quad(\mu_f=+\tfrac{1}{2}).\end{aligned} \tag{B6}$$

In the threshold approximation of Olsson and Turner[11] $A_{\rm CS}(q_1,q_2)$ is symmetric under interchange of q_1 and q_2. Our values for the coefficient of ξ, A_ξ, are real and are given by

$$\begin{aligned}A_\xi&=-0.193\times10^{-4}\quad(\mu_f=-\tfrac{1}{2})\\&=0.484\times10^{-4}\quad(\mu_f=+\tfrac{1}{2}).\end{aligned} \tag{B7}$$

In our calculations we replace A_ξ by the one-pion-exchange ϵ-production diagram of Aaron *et al.*[29]—but *not* using the scattering length approximation for $e^{i\delta_{\pi\pi}}\sin\delta_{\pi\pi}/q_{\pi\pi}$. Call this more general form B_ξ. As discussed in Sec. IV C we must subtract from B_ξ its contribution from the two partial waves $PS11$ and $DP13$ that are being varied in the fitting procedure; call the remainder $\bar{B}_\xi$. We have at the kinematic point under discussion

$$\begin{aligned}B_\xi&=0.105\times10^{-3}+0.285\times10^{-4}i\quad(\mu_f=-\tfrac{1}{2})\\&=-0.263\times10^{-3}-0.713\times10^{-4}i\quad(\mu_i=+\tfrac{1}{2}),\end{aligned} \tag{B8}$$

TABLE XIII. Our results for the $\pi\Delta$ basis function of Eq. (4.4) for the two possible Δ charge states.

Wave	$10^3\, X^{(1)}_{\Delta=\pi^- n}$ $(\mu_i=\frac{1}{2},\ \mu_f=-\frac{1}{2})$	$10^3\, X^{(1)}_{\Delta=\pi^- n}$ $(\mu_i=\frac{1}{2},\ \mu_f=\frac{1}{2})$	$10^3\, X^{(2)}_{\Delta=\pi^+ n}$ $(\mu_i=\frac{1}{2},\ \mu_f=-\frac{1}{2})$	$10^3\, X^{(2)}_{\Delta=\pi^+ n}$ $(\mu_i=\frac{1}{2},\ \mu_f=\frac{1}{2})$
$PP11$	$-0.157-0.607i$	$0.336+1.10i$	$0.223-0.101i$	$0.247-0.376i$
$PP33$	$0.483-0.410i$	$-0.223+2.15i$	$0.571-0.419i$	$-1.27+1.12i$
$DS13$	$-0.397-0.959i$	$-0.723-0.0293i$	$-0.829-0.561i$	$-0.587-0.796i$
$DS33$	$-0.251-0.607i$	$-0.457-0.0186i$	$1.05+0.709i$	$0.742+1.01i$

$$\tilde{B}_\ell = 0.234\times10^{-4} + 0.634\times10^{-5} i \quad (\mu_f=-\tfrac{1}{2})$$
$$= -0.518\times10^{-4} - 0.141\times10^{-4} i \quad (\mu_f=+\tfrac{1}{2}). \tag{B9}$$

The reader should note that the phase of the one-pion-exchange contribution to T in Ref. 29 is not that of Appendix A of this work; B_ℓ is given in Ref. 29, not T_ℓ. He may also note that A_ℓ and B_ℓ are related (approximately) by the factor of -4 of Eq. (4.36b).

APPENDIX C: THE ELASTIC-PRODUCTION-PHASE (EPP) APPROXIMATION

This appendix treats briefly the EPP approximation, which was used to model certain production phases in one of our two fitting procedures. This was done in order to reduce the number of parameters to be determined.

For the case of a single inelastic channel, one may write the elastic amplitude, T_e, and the production amplitude, T_0, as follows:

$$T_e = (K_e - i d_K)/[1 - d_K - i(K_e + K_i)], \tag{C1}$$

$$T_0 = K_0/[1 - d_K - i(K_e + K_i)], \tag{C2}$$

where d_K is given by

$$d_K = K_e K_i - K_0^2 \tag{C3}$$

in terms of the elements of the K matrix

$$K = \begin{pmatrix} K_e & K_0 \\ K_0 & K_i \end{pmatrix}. \tag{C4}$$

We consider here the T's to be the Argand amplitudes, i.e., $T_e = (\eta e^{2i\delta} - 1)/2i$. The phase of T_0 is given by

$$\phi_0 = \tan^{-1}[(K_e + K_i)/(1 - d_K)]. \tag{C5}$$

The phase of T_e is related to ϕ_0 by

$$\phi_e = \phi_0 - \tan^{-1}(d_K/K_e). \tag{C6}$$

The EPP approximation is

$$K_i \ll 1. \tag{C7}$$

Since we expect K_i to be proportional to the production-channel phase-space factor, we expect (C7) to be valid sufficiently close to threshold. Using (C7) in (C1) and (C2), one obtains

$$T_e = (K_e + iK_0^2)/(1 + K_0^2 - iK_e), \tag{C8}$$

$$T_0 = K_0/(1 + K_0^2 - iK_e). \tag{C9}$$

Thus, in this approximation T_0 is related to T_e by

$$T_0 = (1 + iT_e)K_0, \quad \phi_0 \equiv \phi_p. \tag{C10}$$

This is the approximation used in the fitting as an alternative to varying the phase of T_0 independently. We expect it to be valid in the region of the Argand diagram where the elastic amplitude begins to come off the unitarity circle, providing we are not near a resonance.

The approximation of taking the K matrix to be factorizable, which also relates the phases of T_e and T_0, is commonly used in the neighborhood of resonances. It is equivalent to taking all elements of the T matrix to be dominated by a simple pole. In this approximation, we have $d_K \equiv 0$ and the phase ϕ_0 of T_0 is equal to the phase ϕ_e of T_e.

For the energies of the data fit in this work these two approximations give similar predictions for production phases. Consider, for example, the $PP11(\pi\Delta)$ amplitude which, because of the proximity of the highly inelastic 1490 Roper resonance, should be a bounding case. The elastic phase shift at $W = 1375$ MeV is $\delta = 38°$. The phase of the elastic amplitude is $\phi_e = 47°$, while the EPP prediction is $\phi_p = 32°$.

APPENDIX D: STRUCTURE OF THE AXIAL-VECTOR VERTEX FOR $\Delta\pi\Delta$ AND THE GOLDBERGER-TREIMAN RELATION

In this appendix, we extend the Goldberger-Treiman relation to spin-$\frac{3}{2}$ particles. First, however, we must determine the structure of the axial-vector vertex, which we write as

$$\langle \Delta(p') | A^\mu(0) | \Delta(p) \rangle = \bar{u}_\alpha(p') M^{\alpha\beta\mu} u_\beta(p), \tag{D1}$$

where $u_\beta(p)$ is a spin-$\frac{3}{2}$ Rarita-Schwinger tensor and $M^{\alpha\beta\mu}$, a rank-three pseudotensor whose form is to be determined below. Since the spin-$\frac{3}{2}$ particles in (D1) are on the mass shell, the spinors u_β must satisfy the free Dirac equation

$$(\not{p}-m_\Delta)u_\beta(p)=0\,, \tag{D2}$$

and the subsidiary conditions

$$\gamma^\beta u_\beta(p)=0\,,$$
$$p^\beta u_\beta(p)=0\,. \tag{D3}$$

In the determination of $M^{\alpha\beta\mu}$ below, the indices α, β, and μ refer to (D1).

We first consider terms of the form

$$g^{\alpha\beta}g^{\mu\delta},\ g^{\alpha\mu}g^{\beta\delta},\ g^{\beta\mu}g^{\alpha\delta},\ g^{\alpha\delta}g^{\beta\rho}g^{\mu\nu}, \tag{D4}$$

where g is the metric tensor and δ, ρ, and ν are free indices to be contracted with the available four-vectors. There are three linearly independent four-vectors, which we choose to be γ (the Dirac γ matrices), $q=p'-p$ and $P=p'+p$. Of the possibilities represented by the first term in (D4),

$$g^{\alpha\beta}\gamma^\mu\gamma_5,\ \ g^{\alpha\beta}q^\mu\gamma_5 \tag{D5}$$

have the proper parity and G parity. Of the second and third terms only the combination

$$(q^\alpha g^{\mu\beta}+q^\beta g^{\mu\alpha})\gamma_5 \tag{D6}$$

survives G parity, while from the final term, we have

$$q^\alpha q^\beta\gamma^\mu\gamma_5,\ \ q^\alpha q^\beta q^\mu\gamma_5\,. \tag{D7}$$

All other possibilities either violate G parity or are equivalent to some linear combination of the above.

One other remaining possibility is to consider contributions involving the totally antisymmetric tensor ϵ, i.e., terms of the form

$$\epsilon^{\alpha\beta\mu\delta},\ \epsilon^{\alpha\beta\delta\nu}g^{\mu\rho},\ \epsilon^{\alpha\delta\nu\rho}g^{\beta\beta'}g^{\mu\mu'}, \tag{D8}$$

with all possible distinct permutations of superscripts. As mentioned above, there are only three linearly independent four-vectors available for contractions with the free indices in (D8), γ, q, and P. The identity

$$(g^{\alpha\beta}\gamma^\mu-g^{\mu\alpha}\gamma^\beta-g^{\mu\beta}\gamma^\alpha+\gamma^\alpha\gamma^\mu\gamma^\beta)\gamma_5=i\epsilon^{\alpha\beta\mu\rho}\gamma_\rho \tag{D9}$$

(for general α, β, and μ), and the subsidiary conditions (D3) effectively eliminate contractions of ϵ with γ from consideration since they are equivalent to combinations of terms already considered. Furthermore, we know

$$\bar u_\alpha(p')P^\delta\bar u_\beta(p)=\bar u_\alpha(p')(2m_\Delta\gamma^\delta-i\sigma^{\delta\rho}q_\rho)u_\beta(p), \tag{D10}$$

so that contractions of ϵ with P are equivalent to some combination of contractions with γ. Thus, only $\epsilon^{\alpha\beta\mu\delta}q_\delta$ survives, but this has the wrong G parity.

Collecting (D5), (D6), and (D7), we have

$$\langle\Delta(p')|A^\mu(0)|\Delta(p)\rangle=\bar u_\alpha(p')[g_A(q^2)g^{\alpha\beta}\gamma^\mu+h_A(q^2)g^{\alpha\beta}q^\mu$$
$$+f_1(q^2)q^\alpha q^\beta\gamma^\mu+f_2(q^2)q^\alpha q^\beta q^\mu+\tfrac{1}{2}f_3(q^2)(q^\alpha g^{\mu\beta}+q^\beta g^{\mu\alpha})]\gamma_5 u_\beta(p). \tag{D11}$$

Thus we have

$$\lim_{q_\mu\to0}\langle\Delta(p')|\partial_\mu A^\mu(0)|\Delta(p)\rangle$$
$$=i\bar u_\alpha(p')[2m_\Delta g_A(0)g^{\alpha\beta}]\gamma_5 u_\beta(p). \tag{D12}$$

The PCAC hypothesis

$$\partial_\mu A^\mu_\alpha(x)=f_\pi m_\pi^2\phi_\alpha(x)\ \ (\alpha=1,2,3) \tag{D13}$$

leads to

$$g_{\Delta^+\pi^-\Delta^0}=\sqrt{2}\,m_\Delta[g_A(0)]_{\Delta^+\Delta^0}f_\pi \tag{D14}$$

in the limit that the pion four-momentum goes to zero. We have assumed, in the normal fashion, that the matrix element of the axial-vector current is a smoothly varying function of q. A standard quark-model calculation will not support more structure than is present in (D12). Thus, the limit that we have considered ($q^\mu\to0$) enables us to relate the $\Delta\pi\Delta$ coupling constant to a bag-model determination of $(g_A)_{\Delta\Delta}$.

*Present address: 2571 via Campesina, Palos Verdes Estate, CA 90274.

†Address until June, 1980: Strategic Affairs Division, U. S. Arms Control and Disarmament Agency, Washington, D. C. 20451.

[1]A complete compilation of data from these early experiments is given in Ref. 5.

[2]M. De Beer, B. Deler, J. Dolbeau, M. Neveu, Nguyen Thuc Diem, G. Smadja, and G. Valladas, Nucl. Phys. B12, 599 (1969); M. G. Bowler and R. J. Cashmore, *ibid.* B17, 331 (1970); D. H. Saxon, J. H. Mulvey, and W. Chinowsky, Phys. Rev. D 2, 1790 (1970); A. D. Brody, R. J. Cashmore, A. Kernan, D. W. G. S. Leith, B. G. Levi, A. Minten, B. C. Shen, J. P. Berge,

B. Deler, D. J. Herndon, R. Longacre, L. R. Miller, L. R. Price, A. H. Rosenfeld, and P. Söding, *ibid.* 4, 2693 (1971); Y. Williamson, S. Y. Fung, A. Kernan, U. Mehtani, T. L. Schalk, B. C. Shen, W. Michael, R. W. Birge, and G. E. Kalmus, Phys. Rev. Lett. 29, 1353 (1972); J. Dolbeau, M. Neveu, F. A. Triantis, and C. Coutures, Nucl. Phys. B78, 233 (1974); D. C. Jain, Z. Ahmad, and G. Pappas, Phys. Rev. D 15, 3181 (1977); I. Butterworth and K. W. J. Barnham (private communication).

[3]D. H. Saxon, J. M. Mulvey, and W. Chinowsky, Phys. Rev. D 2, 1790 (1970); M. De Beer *et al.*, Nucl. Phys. B12, 599 (1969); J. Dolbeau, M. Neveu, F. A. Triantis, and C. Coutures, *ibid.* B78, 233 (1974).

[4]P. A. M. Gram, F. T. Shively, C. W. Bjork, T. R. King, A. T. Oyer, G. A. Rebka, J. B. Walter, C. A. Bordner, R. Carawon, and E. Lomon, Los Alamos Report No. LA-UR-77-1669, 1977 (unpublished); and (in preparation). We are grateful to Professors Lomon and Rebka for providing us their preliminary results and for helpful conversations.

[5]M. C. Olsson and G. B. Yodh, Phys. Rev. 145, 1309 (1966).

[6]D. J. Herndon, R. Longacre, L. R. Miller, A. H. Rosenfeld, G. Smadja, P. Söding, R. J. Cashmore and D. W. G. S. Leith, Phys. Rev. D 11, 3183 (1975); David J. Herndon, Paul Söding, and Roger J. Cashmore, *ibid.* 11, 3165 (1975).

[7]R. S. Longacre and J. Dolbeau, Nucl. Phys. B122, 493 (1977).

[8]I. Butterworth and K. W. J. Barnham, private communication; K. W. J. Barnham, in *Proceedings of the Topical Conference on Baryon Resonances, Oxford, 1976*, edited by R. T. Ross and D. H. Saxon (Rutherford Laboratory, Chilton, Didcot, England, 1977).

[9]D. E. Novoseller, Nucl. Phys. B137, 509 (1978).

[10]L. N. Chang, Phys. Rev. 162, 1497 (1967).

[11]M. G. Olsson and L. Turner, Phys. Rev. Lett. 20, 1127 (1968); M. G. Olsson, and L. Turner, Phys. Rev. 181, 2141 (1969); M. G. Olsson, E. T. Osypowski, and L. Turner, Phys. Rev. Lett. 38, 296 (1977); 38, 450 (E) (1977); 39, 52 (E) (1977).

[12]W. F. Long and J. S. Kovacs, Phys. Rev. D 1, 1333 (1970).

[13]R. Rockmore, Phys. Rev. Lett. 35, 1408 (1975); Phys. Rev. C 11, 1953 (1975). Footnote 11 of the second reference contains a discussion of the errors in earlier calculations.

[14]E. Lomon, in G. A. Rebka, Jr. *et al.*, LAMPF Research Proposal, 1971 (unpublished).

[15]S. Weinberg, Phys. Rev. 166, 1568 (1968).

[16]S. A. Bunyatov *et al.*, JINR Report No. P1-9668, Dubna, 1967 (unpublished); A. V. Kravtsov *et al.*, Yad. Fiz. 20, 942 (1974).

[17]E. Reya, Rev. Mod. Phys. 46, 545 (1974).

[18]R. Dashen and M. Weinstein, Phys. Rev. 183, 1261 (1969).

[19]J. Schwinger, Phys. Lett. 24B, 473 (1967); J. Schwinger, in *Proceedings of the Seventh Hawaii Topical Conference on Particle Physics, 1977*, edited by J. Okada (University of Hawaii, Honolulu, 1977).

[20]M. L. Goldberger and S. B. Treiman, Phys. Rev. 110, 1178 (1958).

[21]J. Schwinger, Ann. Phys. (N.Y.) 2, 407 (1957); M. Gell-Mann and M. Levy, Nuovo Cimento 16, 705 (1960).

[22]R. Arnowitt, M. H. Friedman, P. Nath, and R. Suitor, Phys. Rev. 175, 1820 (1968).

[23]M. Gell-Mann, R. J. Oakes, and B. Renner, Phys. Rev. 175, 2195 (1968). See Refs. 17 and 24 for comments and criticisms of this work.

[24]J. F. Gunion, P. C. McNamee, and M. D. Scadron, Nucl. Phys. B123, 445 (1977).

[25]R. Arnowitt, M. H. Friedman, P. Nath, and R. Suitor, Phys. Rev. 175, 1802 (1968).

[26]P. Extermann *et al.*, paper submitted to Palermo Conference on High Energy Physics, Palermo, 1975 (unpublished); E. P. Tryon, Phys. Rev. D 10, 1595 (1974); E. W. Beier *et al.*, Phys. Rev. Lett. 30, 399 (1973); L. Rosselet *et al.*, Phys. Rev. D 15, 574 (1977).

[27]G. E. Hite and R. J. Jacob, Nucl. Phys. B134, 291 (1978).

[28]S. Weinberg, Phys. Rev. Lett. 17, 616 (1966).

[29]The generalized isobar model in its canonical form as used in the present analysis was first given by Y. Goradia, LBL Report No. 3628, 1975 (unpublished). See also Ronald Aaron, R. D. Amado, Richard A. Arndt, Yogesh Goradia, Doris C. Teplitz, and Vigdor L. Teplitz, Phys. Rev. D 16, 50 (1977).

[30]V. S. Zidell, R. A. Arndt, and D. A. Roper (unpublished).

[31]J. Franklin, Phys. Rev. D 11, 513 (1975). We approximate Franklin's fit by $\delta = 2.67\tilde{E} - 0.088\,57\tilde{E}^2 + 0.0019\tilde{E}^3$, where $\tilde{E} = (W_3 - 278\ \text{MeV})/10$.

[32]J. M. Blatt and V. F. Weisskopf, *Theoretical Nuclear Physics* (Wiley, New York, 1952), p. 361.

[33]Y. N. Goradia and R. A. Arndt, Phys. Rev. D 19, 2057 (1979).

[34]P. Nath and S. S. Kere, in Lectures from the LAMPF Summer School on Pion-Nucleus Scattering, 1973, edited by W. R. Gibbs and B. F. Gibson [Los Alamos Report No. LA-5443-*C*, 1973 (unpublished)].

[35]K. Johnson and E. C. G. Sudarshan, Ann. Phys. (N.Y.) 13, 126 (1961).

[36]C. R. Hagen, Phys. Rev. D 4, 2204 (1971).

[37]W. Rarita and J. Schwinger, Phys. Rev. 60, 61 (1941).

[38]J. D. Bjorken and S. D. Drell, *Relativistic Quantum Fields* (McGraw-Hill, New York, 1965), p. 377.

[39]L. M. Nath, B. Etemadi, and J. D. Kimel, Phys. Rev. D 3, 2153 (1971).

[40]R. M. Woloshyn, E. J. Moniz, and R. Aaron, Phys. Rev. C 13, 286 (1976).

[41]H. Strubbe, Computer Phys. Commun. 8, 1 (1974).

[42]F. Gursey, A. Pais, and L. A. Radicati, Phys. Rev. Lett. 13, 299 (1964).

[43]B. Sakita and K. C. Wali, Phys. Rev. 139, B1355 (1965).

[44]S. L. Adler and R. F. Dashen, *Current Algebra and Applications to Particle Physics* (Benjamin, New York, 1968), p. 41.

[45]T. DeGrand, R. L. Jaffe, K. Johnson, and J. Kiskis, Phys. Rev. D 12, 2060 (1975). Also see E. Golowich, *ibid.* 12, 2108 (1975); R. H. Hackman, N. G. Deshpande, D. A. Dicus, and V. L. Teplitz, *ibid.* 18, 2537 (1978).

[46]Other theoretical values for $g^2/4\pi$ are 225 ± 60 from D. G. Sutherland, Nuovo Cimento 48, 188 (1967) [see also C. D. Froggatt and N. H. Parsons, J. Phys. G 3, 159 (1977)] using an Adler-Weisberger relation; and 150 from R. P. Feynman *et al.*, Phys. Rev. D 3, 2706 (1971) using a quark model. A recent calculation by H.-O. Kiehlman and W. Schmidt, University of Karlsruhe reports, 1978 (unpublished) using current

superconvergence relations finds $g^2/4\pi \simeq 120$.
[47]R. Kelly (private communication).
[48]K. M. Watson, Phys. Rev. 88, 1163 (1952).
[49]As has been emphasized by S. Weinberg (private communication) virtually nothing is known for certain about the energy dependence of chiral-symmetry-breaking corrections. All determinations of ξ must contend with this uncertainty in the coefficient of ξ.